UNIVERSITA' DEGLI STUDI DI VERONA

DIPARTIMENTO DI SCIENZE DELLA VITA E DELLA RIPRODUZIONE

DOTTORATO DI RICERCA IN BIOSCIENZE

XXIII CICLO

TESI DI DOTTORATO

ENDOPLASMIC RETICULUM STRESS INDUCED BY GEMCITABINE/CANNABINOID COMBINATION TRIGGERS AUTOPHAGY IN PANCREATIC CANCER CELLS THROUGH A ROS MEDIATED MECHANISM

S.S.D. BIO/10 Biochimica

Coordinatore: Prof./ssa Marta Palmieri

Tutor: Prof./ssa Marta Palmieri

Dottorando: Dott./ssa Tatyana Zaniboni

Index

Abstract

English abstract

Gemcitabine (GEM) is currently the standard treatment for advanced pancreatic adenocarcinoma, one of the most aggressive human tumors, although it has a response rate of less than 20%. The purpose of this thesis was to improve GEM activity by addition of cannabinoids, a novel class of antitumor compounds. This work shows that GEM induces both CB1 and CB2 receptors by an NF-κB-dependent mechanism and that its association with cannabinoids synergistically inhibits pancreatic adenocarcinoma cell growth and increases reactive oxygen species (ROS) induced by single treatments. This effect is prevented by the radical scavenger *N*-acetyl-$_L$-cysteine and by the specific NF-κB inhibitor BAY 11-7085, demonstrating that the induction of ROS by GEM/cannabinoids and of NF-κB by GEM is required for the antiproliferative synergism. Neither apoptotic nor cytostatic mechanisms are responsible for the synergistic cell growth inhibition, which is strictly associated to the enhancement of endoplasmic reticulum stress and autophagic cell death. . Noteworthy, the antiproliferative synergism is stronger in GEM-resistant compared to GEM-sensitive pancreatic cancer cell lines and no synergism is observed in normal primary fibroblasts. The combined treatment strongly inhibits growth of human pancreatic tumor cells xenografted in nude mice without apparent toxic effects.

Italian abstract

Gemcitabina (GEM) è attualmente il chemioterapico standard per il trattamento dell'adenocarcinoma pancreatico, anche se ha un tasso di risposta inferiore al 20%. Lo scopo di questa tesi è stato quello di migliorare l'attività della GEM con l'aggiunta di cannabinoidi, una nuova classe di composti antitumorali. Questo lavoro mostra che GEM è in grado di indurre entrambi i recettori dei cannabinoidi CB1 e CB2 tramite un meccanismo NF-κB-dipendente e che la sua associazione coi cannabinoidi inibisce sinergisticamente la crescita di cellule di adenocarcinoma pancreatico aumentando le specie reattive dell'ossigeno (ROS) indotte dai singoli trattamenti. Questo effetto è inibito dall'antiossidante *N*-acetyl-L-cysteine e dallo specifico inibitore di NF-κB, BAY 11-7085, dimostrando che l'induzione di ROS dalla combinazione GEM/cannabinoidi e di NF-κB da GEM è richiesta per la sinergia antiproliferativa. Né meccanismi apoptotici né citostatici sono responsabili della inibizione sinergica della crescita cellulare, che risulta invece strettamente associata all'aumento di stress del reticolo e alla morte cellulare autofagica.

La sinergia antiproliferativa è più forte nelle linee cellulari di pancreas resistenti alla GEM rispetto a quelle più sensibili e nessuna sinergia si osserva nei fibroblasti primari normali.

Il trattamento combinato inibisce fortemente la crescita di cellule tumorali di pancreas umane xenotrapiantate in topi nudi senza apparenti effetti tossici.

.

Introduction

Introduction

Pancreas anatomy and physiology

The pancreas, an organ of endodermal derivation, is the key regulator of protein and carbohydrate digestion and glucose homeostasis.

The exocrine pancreas (80% of the tissue mass of the organ) is composed of a branching network of acinar and duct cells that produce and deliver digestive zymogens into the gastrointestinal tract. The acinar cells, which are organized in functional units along the duct network, synthesize and secrete zymogens into the ductal lumen in response to cues from the stomach and duodenum. Within the acinar units near the ducts are centroacinar cells.

The endocrine pancreas, which regulates metabolism and glucose homeostasis through the secretion of hormones into the bloodstream, is composed of four specialized endocrine cell types gathered together into clusters called Islets of Langerhans.

Mirroring the physiologic and cellular diversity of the pancreas is a spectrum of distinct pancreatic malignancies that possess histological and molecular features that recall the characteristics of the various normal cellular constituents. These multiple tumor types and hallmark features are summarized in Table 1. Pancreatic ductal adenocarcinoma (PDAC), whose nomenclature derives from its histological resemblance to ductal cells, is the most common pancreatic neoplasm and accounts for >85% of pancreatic tumor cases [2].

Pancreatic neoplasm	Histological features	Common genetic alteration
Ductal adenocarcinoma	Ductal morphology; desmoplasia	*K-RAS, p16INK4a, TP53, SMAD4*

Variants of ductal adenocarcinoma
  a. Medullary carcinoma
  b. Colloid (mucinous noncystic) carcinoma
	Poorly differentiated; intratumoral lymphocytes
	Mucin pools
		hMLH1, hMSH2
		MUC2
		overexpression

Acinar cell carcinoma	Zymogen granules	*APC/β-catenin*
Pancreatoblastoma	Squamoid nests, multilineage differentiation	*APC/β-catenin*
Solid pseudopapillary neoplasm	"Pseudo" papillae, solid and cystic areas, hyaline globules	*APC/β-catenin;* *CD10 expression*
Serous cystadenoma	Multilocular cysts; glycogen-rich epithelium	VHL
Pancreatic endocrine tumors	Hormone production	MEN1

Table 1: pancreatic tumors and associated genetic alterations

Pancreatic Adenocarcinoma

Pancreatic adenocarcinoma (PDAC) is one of the most aggressive and devastating human malignancies with a death-to-incidence ratio of 0.99 [3]. Although it represents only 2-3% of all cancers [4], pancreatic adenocarcinoma is the 4th cause of death by cancer after lung, prostate (breast in women), and colorectal cancers since 1970s.

PDAC is associated with only a few known demographic and environmental risk factors and a handful of autosomal dominant genetic conditions. Multiple studies have established advanced age, smoking, and long-standing chronic pancreatitis as clear risk factors; diabetes and obesity also appear to confer increased risk. Increased risk has also been documented in relatives of PDAC patients, and it is estimated that

10% of PDAC cases are associated with an inherited predisposition based on familial clustering [2].

Molecular genetics of PDAC

Many advances have been made over the past 2 decades in the characterization of the molecular alterations that take place in pancreatic cancer.

These may be classified as alterations in:

- oncogenes,
- tumor suppressor genes,
- growth factors.

Oncogenes

Certain genes exhibit increased biologic activity as a result of mutation and are termed oncogenes. The oncogene most commonly detected in human cancers is the RAS gene. Not surprisingly, the RAS gene is also the most important oncogene identified to date in pancreatic cancer. It comprises 3 families, H-RAS, K-RAS, and N-RAS. Of these, the K-RAS family is responsible for almost all of the pancreatic cancer mutations, with mutations in the other families occurring only rarely.

The gene encodes p21, a membrane-associated guanine nucleotide binding signal transduction protein that regulates many cellular functions, including cell growth, proliferation, and differentiation. Studies suggest that K-RAS, which is located on chromosome 12p13, is mutated in up to 95% of pancreatic adenocarcinomas. These mutations, thought to be an early event in the pathogenesis of pancreatic carcinoma, are point mutations. These mutations in the K-ras gene result in a constitutively active GDP-bound product that promotes increased signal transduction and uncontrolled growth [5].

Tumor suppressor genes

Inactivation of this class of genes results in the elimination of vital negative regulators of cell proliferation allowing for uncontrolled growth. A growing number

of tumor suppressor genes have been identified in the pathogenesis of pancreatic cancer:

- p53,
- members of the INK4 family,
- DPC4/SMAD4.

The p53 tumor suppressor gene is located on chromosome 17p. It encodes a 53-kD nuclear phosphoprotein that acts as a transcription factor capable of modulating the expression of an array of genes involved in critical functions, including cell cycle regulation, arrest, apoptosis, differentiation, DNA surveillance, and repair.

p53 is thought to be mutated in anywhere between 40% and 100% of cases and constitutes the most commonly mutated tumor suppressor gene in pancreatic cancer.

The p16 tumor suppressor gene was the first member to be identified in the INK4 family of cyclin-dependent kinase (CDK) inhibitors. It is located on chromosome 9p and has been implicated in a variety of tumors, including pancreatic cancer. The p16 gene product normally binds to the cyclin CDK4 complex and prevents it from phosphorylating the retinoblastoma protein (RB). In its nonphosphorylated state, the RB protein arrests the cell cycle at the G1/S checkpoint. It does so by forming a complex with E2F and, by sequestering it, preventing it from acting as a transcription factor that allows for the progression of the cell cycle into the S phase. Loss of p16 activity results in no inhibition at the level of the cyclin-CDK4 complex and allows for uncontrolled growth. Studies suggest that p16 activity is lost in about 40% of pancreatic cancers by homozygous deletion.

Growth Factors

Various growth factors and their receptors have been implicated as modifying the level of aggression of pancreatic cancer and influencing the clinical course of the disease.

The FGF (fibroblast growth factors) family consists of 19 homologous polypeptide growth factors that participate in a host of essential cell functions, including cell differentiation during tissue repair, mitogenesis, and angiogenesis. FGF-1-5 and 7 have been found to be overexpressed in certain human pancreatic cancer cell lines.

Furthermore, most human pancreatic cancers have been shown to overexpress one (FGFR-1β) of the high affinity transmembrane tyrosine kinase receptors that function as signal molecules to mediate the effects of FGF. Upon binding a ligand, the FGF receptor homo- and heterodimerizes. It then transphosphorylates tyrosine residues located on its intracellular domain, which allows for signal transmission via one of various cascades. These include the phosphatidyl-inositol-3 kinase, the ras, raf, and MAP kinases. Which one is employed depends on the cell type, the types of receptors in the heterodimer, and the nature of the ligand.

Activated MAP kinases then translocate to the nucleus where they induce oncogenes such as fos and jun, leading to cell proliferation. Some studies have reported increased levels of FGFR as well as closely related receptors such as HER 2 and HER 3 in human pancreatic cancer [1, 6]. Furthermore, it is also known that several ligands for the FGF receptor such as EGF, tumor growth factor- β (TGF- β), and heparin binding EGF-like growth factor (HB-EGF) are also overexpressed in pancreatic cancer. It has been proposed that this receptor-ligand system plays a role in pancreatic carcinogenesis via autocrine and paracrine mechanisms.

Other growth factors that may play a role in pancreatic cancer include insulin-like growth factor (IGF), platelet-derived growth factor (PDGF), vascular endothelial growth factor (VEGF), and hepatocyte growth factor (HGF) [5].

Chemotherapy approach

Up to now, despite decades of efforts at elucidating molecular pathways involved in initiation and progression and at identifying effective therapies, the prognosis of pancreatic adenocarcinoma has not improved. At diagnosis, less than 20% of patients are candidates for surgery with curative intent [7].

Standard treatments for advanced disease and for adjuvant and neo-adjuvant regimens include radiotherapy and/or chemotherapy. Radiotherapy has been shown to have some utility for regional confined cancers, but is often too toxic for tissues surrounding the neoplasia. Monotherapy with gemcitabine (GEM) has been the

standard treatment during the last decade, although it has a response rate of less than 20% [8].

The cytosine analogue Gemcitabine (2',2'-difluorudeoxycytidine, dFdC; GEM) is an S-phase nucleoside that is currently considered to be the single agent of choice in advanced pancreatic cancer.
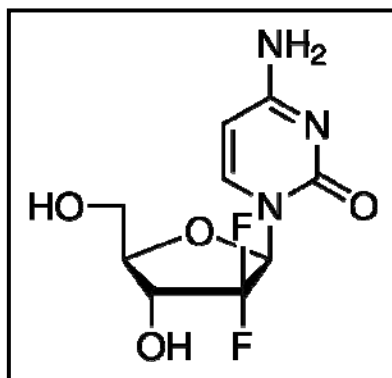

Figure 1: structure of GEM

GEM (Figure 1) has three mechanisms of action:

1. competes for incorporation into DNA, thereby inhibiting the synthesis of DNA;
2. prevents DNA repair by masked termination;
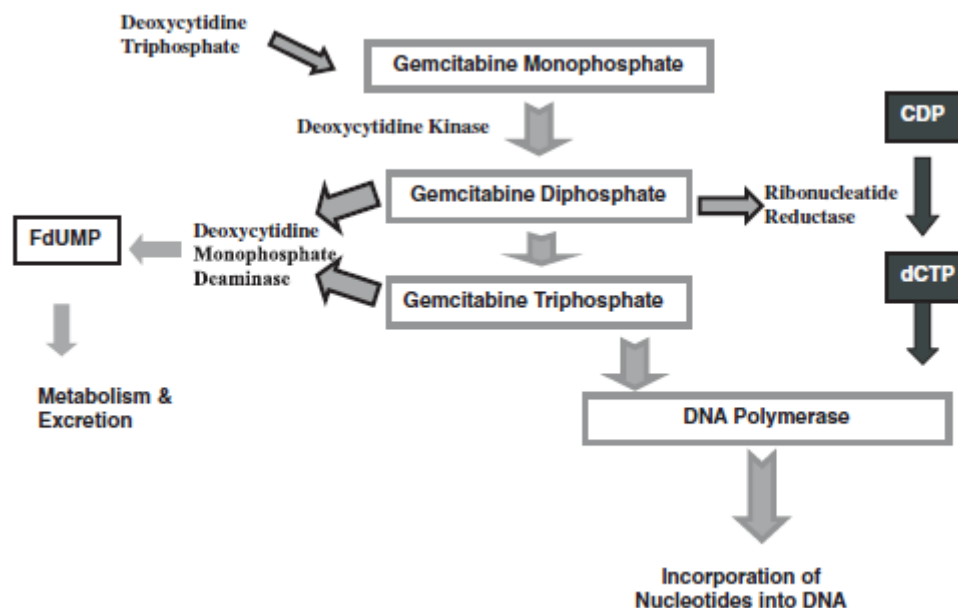3. undergoes self-potentiation.

Figure 2: mode of action of GEM.

GEM undergoes phosphorylation by deoxycytidine kinase to difluorodeoxycytidine di- then tri-phosphate. GEM diphosphate inhibits ribonucleotide reductase, which is the primary enzyme involved in the formation of deoxycytidine monophosphate, a natural substrate in DNA replication. This allows the incorporation of gemcitabine triphosphate nucleotides into the DNA chain during replication.

GEM permits one more nucleotide to pair before termination of the replication process. This means that the GEM nucleotide is less susceptible to excision repair by exonuclease enzymes, making DNA repair more difficult (masked termination).

GEM also perpetuates its own activity and survival by reducing deoxycytidine triphosphate inhibition of deoxycytidine kinase (which phosphorylates GEM) and inhibiting deoxycytidine monophosphate deaminase (normally integral in GEM degradation). Deoxycytidine monophosphate deaminase is inhibited directly by GEM triphosphate and indirectly inhibited by GEM diphosphate.

GEM has shown a 5–11% response rate for advanced pancreatic cancer, with a median survival rate of 5.7–6.3 months in Phase I and II studies. In the pivotal Phase III trial the median survival was increased from 4.4 months using bolus i.v. 5-FU (63 patients) to 5.7 months with GEM (63 patients), and the one-year survival was increased from 2% to 18%, respectively [9].

Many clinical trials have failed to demonstrate an improvement in overall survival (OS) with the addition of different drugs to GEM, including cetuximab and bevacizumab. Nevertheless, some modest but interesting advances have been provided by drug combination therapies such as GEM-erlotinib, GEM-capecitabine, and GEM plus a platinum salt [7]. Nowadays, research is focused on the identification of other potential targets of response, the regulation of which may improve GEM antitumoral activity, which does provide a modest improvement in the quality of life [8].

Reactive oxygen species

Reactive oxygen species (ROS) are chemically-reactive molecules containing oxygen. Examples include free radicals such as superoxide ($O_2 \cdot$ -), hydroxyl radical (OH·), and non-radical molecules, such as hydrogen peroxide (H_2O_2).

Various pathways of ROS formation exist. The production of superoxide occurs mostly within the mitochondria of a cell. The mitochondrial electron transport chain is the main source of ATP in the mammalian cell and thus is essential for life. During energy transduction, a small number of electrons "leak" to oxygen prematurely, forming the oxygen free radical superoxide. Mitochondria, in fact, are considered the major source of cellular production of ROS: it is estimated that 2% of consumed oxygen reacts with electrons that escape from the respiratory chain, produces superoxide ion, and is then converted into hydrogen peroxide. An excess of ROS causes oxidative stress that leads to the activation of many cellular antioxidant systems (eg. superoxide dismutase, catalase, glutathione system, thioredoxin) in order to avoid damage to DNA, proteins and lipids [10].

The ROS production correlates with normal cell proliferation through activation of growth-related signalling pathways. Indeed, exposure to low levels of ROS can increase growth of many types of mammalian cells, whereas scavengers of ROS suppress normal cell proliferation in human and rodent fibroblasts.

Furthermore, growth factors trigger hydrogen peroxide (H_2O_2) production that leads to mitogen-activated protein kinase activation and DNA synthesis, a phenomenon

inhibited by antioxidant molecules. Several observations suggest that ROS also participate in carcinogenesis:

1. ROS production is increased in cancer cells and an oxidative stress can induce DNA damages that lead to genomic instability and possibly stimulate cancer progression;

2. elevated ROS levels are responsible for constant activation of transcription factors, during tumor progression.

Whereas, under certain circumstances, ROS promote cell proliferation, they can also induce apoptosis. Indeed, most anticancer drugs kill their target cells at least in part through the generation of elevated amounts of intracellular ROS. ROS can stimulate proapoptotic signal molecules, such as apoptosis signal regulating kinase 1, c-Jun-NH2-kinase, and p38; activate the p53 protein pathway; or engage the mitochondrial apoptotic cascade. The various ROS can exert different effects according to their nature and to their intracellular level, which is determined by both their production rate and the activity of antioxidant enzymes.

More recent studies have shown that cancer cells have a level of ROS higher than normal cells, associated with oncogenic stimulation, alterations in metabolic and mitochondrial malfunction. The consequences of increased oxidative stress are the stimulation of proliferation, the increase in mutations and genetic instability [1]. The intrinsic oxidative stress of cancer cells is a feature that can be exploited therapeutically. Because cancer cells produce high levels of ROS and are under increased oxidative stress, it is reasonable to speculate that compared to normal cells, the malignant cells would be more dependent on antioxidant enzymes and other antioxidant defense systems to cope with such stress. It follows that inhibition of antioxidant enzymes or exposure to further exogenous ROS insults would cause more ROS-mediated damage in cancer cells than in normal cells [6]. This model was also confirmed by our group on pancreatic adenocarcinoma cells and normal human fibroblasts following treatment with the oxidant DEM (DiEthyl Maleate), a known oxidant agent). DEM inhibited the growth of adenocarcinoma cell lines in a dose dependent manner, while it was ineffective on normal human fibroblasts.
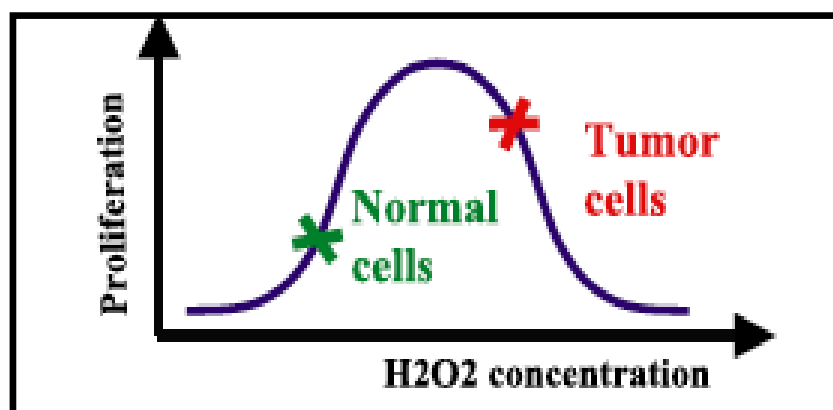
Figure 3: model proposed to explain the opposite effects of various concentrations of intracellular H_2O_2 on cellular proliferation of nontransformed and tumor cells [1].

Gemcitabine and ROS

Recently, our research group showed that GEM induces an approximately 2-fold increase of intracellular free radicals and that 1 mM of the radical scavenger NAC (N-acetyl-L-cysteine) is able to rescue, at least in part, the antiproliferative effect of GEM. Moreover, a positive correlation was found between the intrinsic ROS stress and the sensitivity to GEM in 10 pancreatic adenocarcinoma cell lines (Table 2 and Fig 4) [11, 12].

Cell lines	Origin	IC$_{50}$ GEM (nM) 48h	RMF
PSN1	Primary	8	30.2
PC1J	Primary	30	31
PT45P1	Primary	50	60.9
MiaPaCa2	Primary	90	50.8
PaCa3	Primary	220	4.7
PaCa44	Primary	250	3.2
Panc1	Primary	200	2.4
CFPAC1	Metastasis (liver)	9.5	57.1
T3M4	Metastasis (node)	25	48.6
HPAFII	Metastasis (ascites)	40	35.4

Table 2: IC$_{50}$ value of 48h GEM and relative mean fluorescence (RMF) of pancreatic adenocarcinoma cell lines. Relative mean fluorescence is the ratio between fluorescence intensity of cells treated and untreated (autofluorescence) with 2',7'-dichlorofluorescein (DCF) and correspond to the basal level of ROS.
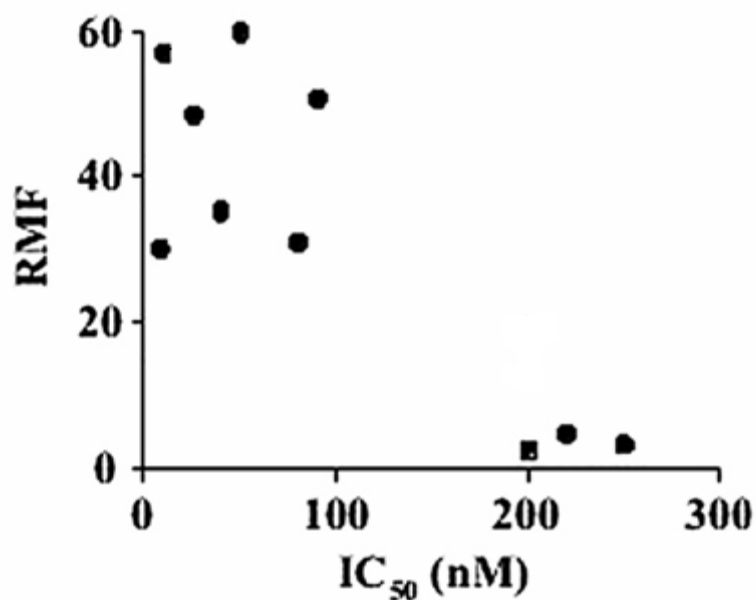

Figure 4: RMF versus IC$_{50}$.

The different levels of ROS in normal and tumor cells may allow a selective action of chemotherapy to the cancer cells. This effect might be achieved by combining GEM with one or more oxidizing agents to further increase intracellular oxidative stress of cancer cells.

Cannabinoids

Cannabis has been used for many years and for many different purposes (i.e. fiber, medicinal, ...). However, the endocannabinoid signaling system has only recently been the focus of medical research and considered a potential therapeutic target [13]. At the present time, three general types of cannabinoids have been described :

- *phytocannabinoids* occur uniquely in the cannabis plant;
- *endogenous cannabinoids* are produced in the bodies of humans and other animals;
- *synthetic cannabinoids* are similar compounds produced in a laboratory.

Phytocannabinoids, also called *natural cannabinoids*, *herbal cannabinoids*, and *classical cannabinoids*, are only known to occur naturally in significant quantity in the cannabis plant, and are concentrated in a viscous resin that is produced in glandular structures known as trichomes. In addition to cannabinoids, the resin is rich in terpenes, which are largely responsible for the odour of the cannabis plant.

Phytocannabinoids are nearly insoluble in water but are soluble in lipids, alcohols, and other non-polar organic solvents. However, as phenols, they form more water-soluble phenolate salts under strongly alkaline conditions.

All natural cannabinoids are derived from their respective 2-carboxylic acids (2-COOH) by decarboxylation (catalyzed by heat, light, or alkaline conditions).

At least 70 cannabinoids have been isolated from the cannabis plant. Tetrahydrocannabinol (THC), cannabidiol (CBD) and cannabinol (CBN) are the most prevalent natural cannabinoids and have received the most study.

Endocannabinoids mimic the pharmacological actions of the psychoactive principle of marijuana, Δ_9 tetrahydrocannabinol (Δ_9-THC). Endocannabinoids are endogenous lipid signaling molecules. They are generated in the cell membrane from phospholipid precursors and possess cannabimimetic properties because they bind and activate one or more cannabinoid receptor subtypes. Endocannabinoids are implicated in different physiological and pathological functions (regulation of food intake, immunomodulation, inflammation, analgesia, cancer, addictive behavior, epilepsy and others). The two best-studied endocannabinoids isolated to date are arachidonoylethanolamine (anandamide or AEA) and 2-arachidonoylglycerol (2-AG). AEA is hydrolyzed by the enzyme fatty-acid amide hydrolase (FAAH) whereas 2-AG is degraded by the enzyme monoacylglycerol lipase (MGL).

Synthetic cannabinoids are particularly useful in experiments to determine the relationship between the structure and activity of cannabinoid compounds, by making systematic, incremental modifications of cannabinoid molecules. Laboratory synthesis of cannabinoids was often based on the structure of herbal cannabinoids, and a large number of analogues have been produced and tested.
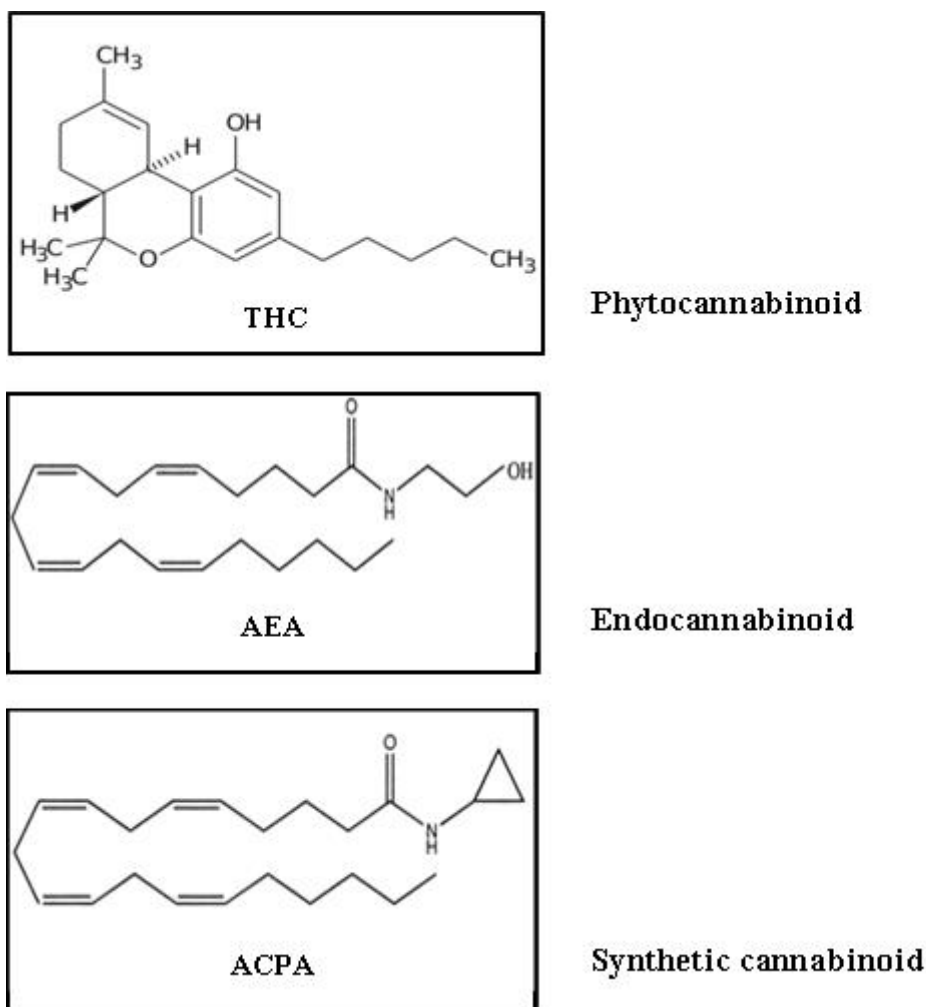
Figure 5: types of cannabinoids.

Cannabinoid receptors

Cannabinoids produce their effects through the activation of distinct G protein-coupled receptors identified as the cannabinoid CB1 and CB2 receptors. These are members of the superfamily of seven-transmembrane-spanning G protein-coupled receptors and share 44% identity at the protein level. Similarity increases to 68% when only the transmembrane region is considered. Activation of both cannabinoid receptor subtypes inhibits adenylate cyclase activity by coupling to the α–subunit of the G protein of the Gi/o family (Gi 1, 2 and 3, and Go 1 and 2).

In contrast to CB2 receptor activation, CB1 receptor activation modulates calcium or potassium conductance, property linked to the suppression of neuronal excitability

and neurotransmitter release. However, activation of MAPK and Krox-24 expression presumably through the activation of G-protein $\beta\gamma$ subunits is another signalling mechanism recruited by both CB1 and CB2 receptors. Furthermore, CB1 receptor activation can inhibit type 5-HT3 ion channels, modulate the production of nitric oxide, alter sodium channel conductance and activate the Na^+/H^+ exchanger [13].

The **CB1 receptor** was first cloned in 1990 from a cortical rat brain cDNA library, this was followed by the cloning of human and mouse analogues. These encode proteins of 427 (human) and 473 (rat) amino acids and have 97–99% amino acid sequence homology across species [14]. CB1 receptors are found mainly in the CNS and, to a lesser extent, in certain peripheral tissues. At the peripheral level, they are localized in adrenal gland, adipose tissue, heart, liver, lung, prostate, uterus, ovary, testis, bone marrow, thymus, tonsils and presynaptic nerve terminals. Within the brain, they are found in the cerebral cortex, hippocampus (with highest concentrations in the dentate gyrus), amygdala, basal ganglia, substantia nigra pars reticulata, internal and external segment of the globus pallidus and cerebellum (molecular layer). The distribution of cannabinoid receptors provides an anatomical basis for the analgesic effects of the cannabinoids. Activation of presynaptic CB1 receptors in different brain regions or on primary afferents inhibits the release of neurotransmitters by decreasing calcium conductance and by increasing the potassium conductance [13].

CB2 receptors are primarily localized to cells of the immune system. The CB2 receptor was cloned in 1993 from human promyelocitic HL-60 cells. This gene encodes a protein of 360 amino acids, and is only 48% homologous to CB1 [14]. CB2 receptors are mainly found in the spleen, tonsils and thymus, tissues responsible for immune cell production and regulation. These immune cells include mast cells, B cells, T4 and T8 cells, microglial cells, macrophages, natural killer cells and, to a lesser extent, monocytes and polymorphonuclear neutrophils. Previous reports suggested that CB2 receptors were absent in neurons of the central nervous system (CNS). However, recent studies suggest that they are found in the brain, on dorsal

root ganglia, in the lumbar spinal cord, on sensory neurons, on microglia as well as in peripheral tissues.

A better understanding of the role of cannabinoid receptors in different physiological processes has been obtained through research employing pharmacological and genetic tools such knockout mice with disrupted CB1 and/or CB2 genes [13]. The role of the CB1 receptor in the central effect of cannabinoids was investigated by measuring the response of CB1$^{+/+}$ and CB1$^{-/-}$ mice to THC in different assay. These experiment have shown that the main pharmacological effect of THC are mediated by the CB1 receptor [15]. The same experiment was performed for tested if the immune effects are mediated by cannabinoid CB$_2$ receptors. Were evaluated the immunomodulatory effects of cannabinoids in cannabinoid CB$_2$ receptor deficient mice using a T cell co-stimulation assay. THC inhibits helper T cell activation through macrophages derived from wild type, but not from knockout mice, thus indicating that this effect is mediated by the cannabinoid CB$_2$ receptor [16].
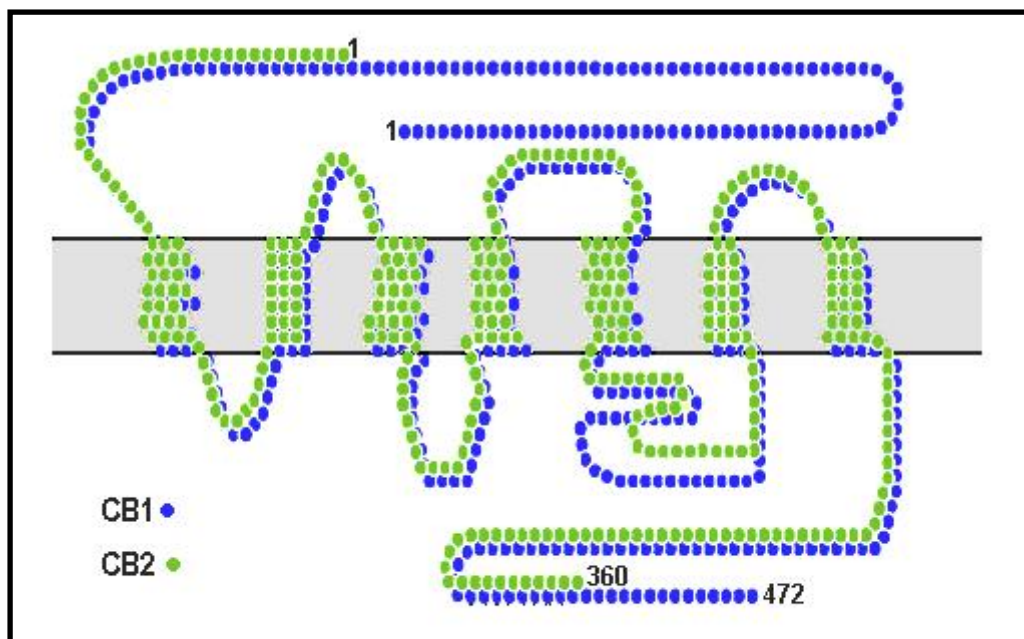

Figure 6: structure of cannabinoid receptors

Antitumoral action of cannabinoids

Cannabinoids have been successfully used in the treatment of some of the side effects, such as nausea and vomiting, weight loss, lack of appetite and pain that often accompany cancer. Δ9-THC (Dronabinol) and LY109514 (Nabilone) are approved to treat nausea and vomiting associated with cancer chemotherapy. Although cannabinoids are used in the palliative treatment of cancer, they are not yet used as a treatment for tumor progression itself. However, the first study to show that cannabinoids had anti-tumor effects was reported by Munson et al. in 1975. They demonstrated that administration of Δ^9-THC, Δ^8-THC and cannabinol inhibited the growth of Lewis lung adenocarcinoma cell growth in vitro, and in vivo after oral administration to mice. Since then, cannabinoids have been shown to have anti-proliferative, anti-metastatic, anti-angiogenic and pro-apoptotic effects in various cancer types (lung, glioma, thyroid, lymphoma, skin, pancreas, uterus, breast and prostate carcinoma) using both in vitro and in vivo models. Recently, more evidence has been obtained that suggests that phyto, endo- and synthetic cannabinoids could be useful in the treatment of cancer due to their ability to regulate cellular signalling pathways critical for cell growth and survival [14].

Recent findings have also shown that the ER stress–evoked upregulation of the p8/TRB3 pathway induced autophagy via inhibition of the Akt/mTORC1 axis and that activation of autophagy promoted the apoptotic death of tumor cells [17].

The majority of the literature demonstrates that various cannabinoids inhibit cancer cell growth in vitro and tumor growth in vivo and that the induction of apoptosis plays a major role in the mechanism for this effect. The potency of this effect varies with each cannabinoid. Therefore, the differences in binding properties at the cannabinoid receptors may result in different downstream effects. For example, partial agonism at the cannabinoid receptors by Δ^9-THC or AEA compared to potent full agonism at the cannabinoid receptors by the synthetic cannabinoids JWH-133 or WIN 55,212-2, could lead to a divergence of downstream signaling that could produce altered responses in cell growth. The full potential of these synthetic cannabinoids has yet to be determined and there is a need for much more extensive research into the dose-response relationships as well as the mechanisms elicited by

the specific cannabinoids if cannabinoids are going to be further developed into potential cancer treatments [14].

Autophagy

During the genesis of cancer, tumour cells experience various forms of intracellular and extracellular stress. This hostile situation results in damage to cellular proteins, the production of reactive oxygen species (ROS) and the replication of cells with heritable DNA damage. Tumour cells must therefore utilise homeostatic mechanisms in order to maintain sufficient energy and integrity in order to survive.

Macroautophagy (hereafter referred to autophagy for simplicity) is one process within the cell that can serve to support these demands, through the lysosomal-mediated degradation of cellular proteins and organelles. This not only results in the removal of damaged cellular constituents, but also, where required, can provide the catabolic intermediates for intracellular production of ATP when exogenous energy supplies are limited.

However, although a clear role in cell survival undoubtedly exists, evidence also points to a tumour-suppressive role: downregulation of several autophagy genes occurs in human cancer, mouse models where critical autophagy regulators have been deleted support a role for autophagy in tumour suppression, and autophagy has been implicated in cell death and oncogene-induced senescence.

Autophagy when translated from the Greek, that literally means 'self-eating', comprises a multistep process of sequestration and subsequent degradation of intracellular material within specialised compartments.

Autophagy is orchestrated by a subset of genes that were originally identified in yeast and are called autophagy-related genes (ATG), many of which have mammalian orthologues [18].

Autophagy can be divided into different stages:
1. initiation;
2. autophagosome formation (nucleation, elongation and completion);
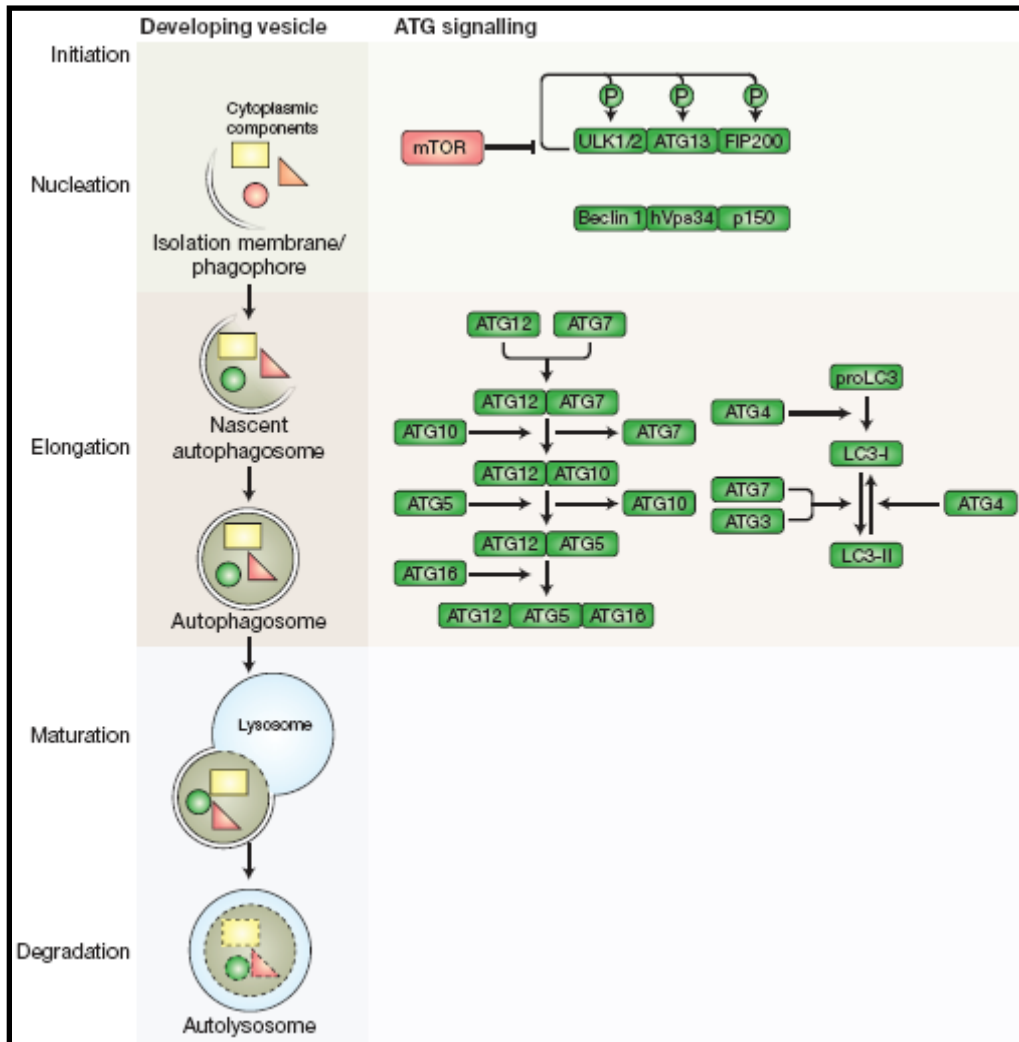
3. maturation;

4. degradation.

Figure 7: autophagy stages

Initiation

Initiation in mammalian cells starts with the activation of a serine/threonine kinase complex that contains ULK1/2 (orthologues of the yeast protein Atg1), ATG13 and FIP200. This complex transfers signals from the nutrient-sensing mTOR kinase (MTOR; mammalian/mechanistic target of rapamycin) to initiate autophagy. Inhibition of mTOR-induced phosphorylation of ULK and ATG13 liberates the kinase activity of ULK, which subsequently phosphorylates itself, ATG13 and

FIP200. The ULK complex then accumulates at the initiating focus of vesicle formation: the isolation membrane or phagophore [18].

Autophagosome formation

Vesicle nucleation depends on the activity of the class III phosphoinositide 3-kinase (PI3K-III), hVps34 (the orthologue of yeast Vps34) and its formation of a complex with Beclin 1 (yeast Atg6) and p150/hVps35 [19, 20]. Vesicle elongation and completion from the isolation membrane/phagophore to a nascent autophagosome and the completed, closed autophagosome is mediated by two ubiquitin like conjugation systems: the ATG12 and ATG8 conjugation systems [18]. The ubiquitin-like ATG12 is activated by ATG7 and then temporarily binds to the E2-like enzyme ATG10 before being transferred to ATG5. ATG5 further reacts with ATG16 to form a multimeric complex of ATG12–ATG5–ATG16 [21, 22].

LC3 is synthesised as a precursor protein proLC3 and is immediately processed to LC3-I by ATG4 through cleavage of the C-terminal amino acid. LC3 maturation completes with the reversible conjugation of LC3-I to phosphatidylethanolamine (PE) at the C-terminus by ATG3 and ATG7 to form LC3-II on the surface of autophagosomes [21, 22].

Both the ATG12–ATG5–ATG16 complex and LC3-II are essential for autophagy. The ATG12–ATG5–ATG16 complex is required for targeting of LC3 to the autophagosomal membrane and accelerated conjugation of LC3 to PE.

Maturation and degradation

The maturation process encompasses the fusion of autophagosomes with lysosomes to form the end-stage vesicle of autophagy: the autolysosome.

Molecular mechanisms of autophagosome maturation are only recently emerging and involve the actions of lysosomal proteins LAMP1 and LAMP2, the small GTPase Rab7 (RAB7A) and UVRAG (the protein product of the ultraviolet-radiation-resistance-associated gene) [23]. The tumour suppressor UVRAG not only regulates the interaction of Beclin 1 and hVps34 at the stage of vesicle nucleation but also

plays an important role in the maturation step. UVRAG directs so-called tethering proteins (i.e. proteins that connect the autophagosome to its target) to the autophagosomal membrane and thereby activates Rab7 to facilitate fusion with lysosomes [19]. The final autolysosome is an acidic vesicle wherein the intracellular material gets degraded by lysosomal hydrolases, especially cathepsins.

Amino acids and other constituent parts generated in this catabolic process are then released from the autolysosome to fuel cellular resources.

ER-stress

The endoplasmic reticulum (ER) is an organelle with crucial biosynthetic and signaling functions in eukaryotic cells. The ER is not only the major intracellular calcium (Ca^{2+}) storage organelle critically involved in Ca^{2+} homeostasis and Ca^{2+} mediated signaling pathways, but it also provides the environment for the synthesis, folding, and modification of proteins destined to be secreted or embedded in the plasma membrane. Moreover, the ER is the major site for the biosynthesis of steroids, cholesterol, and lipids. Proper folding, maturation, and stabilization of the nascent protein in the ER require the highly oxidizing and Ca^{2+}-rich ER environment, which is essential for the different post translational and cotranslational modifications, including glycosylation and disulfide bridge formation, to which proteins are subjected after entering the ER. These processes are assisted and monitored by several resident chaperones and Ca^{2+} binding proteins, including the glucose-regulated proteins such as GRP78, BiP, calreticulin and calnexin, and several folding enzymes, such as the thioredoxin-like protein disulfide isomerase (PDI).

Proteins that fail to adopt a correctly folded or native conformation, or a proper oligomeric assembly in case of multisubunit proteins, are retrotranslocated to the cytosol through a process known as ER-associated protein degradation (ERAD), and further degraded by the 26S proteasome.

The term 'endoplasmic reticulum stress' defines any perturbation that compromises the protein folding functionality of the ER [24].

The ER-stress response is generally activated in response to various stressful conditions, such as hypoxia, low glucose levels, alterations of calcium homeostasis, the accumulation of misfolded proteins, and others. Several of these conditions are particularly relevant in tumor cells. For instance, the vigorous growth of tumors may expose cells at the frontline of expansion to regions with insufficient blood supply and therefore low oxygen and glucose availability. The latter condition is further exacerbated by the general metabolic phenotype of tumor cells that shifts the emphasis of sugar breakdown from oxidative phosphorylation to ''aerobic glycolysis'' (Warburg effect), necessitating the increase of sugar consumption. In addition, highly proliferative growth, in particular when combined with a secretory phenotype such as is present in multiple myeloma or prostate carcinoma cells, requires revved up protein synthesis and therefore leads to the accumulation of misfolded, damaged, and other garbage proteins as byproducts . As illustrated in Fig. 6, all of these conditions are known to trigger the ER-stress response (also called the unfolded protein response, UPR, when the causative trigger relates to misfolded/unfolded proteins) [25].
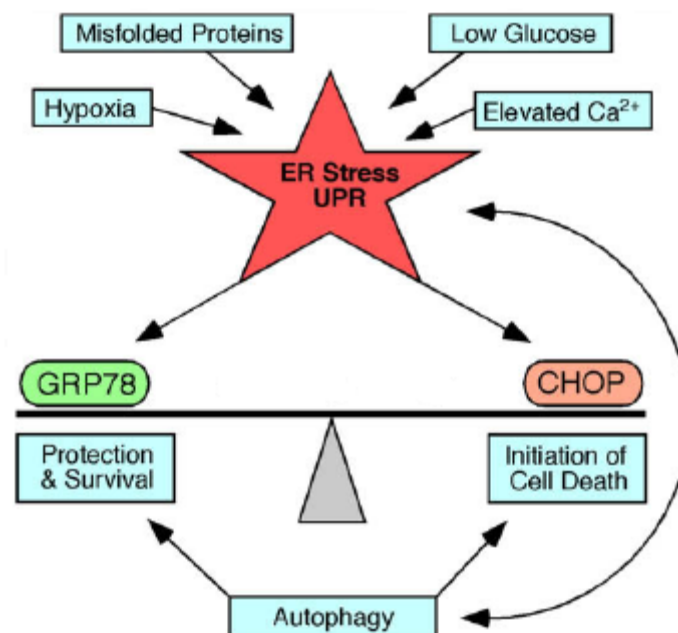

Figure 8: Simplified description of the ER stress.

The initial effort of the ER-stress response is to protect the stressed cells by reestablishing homeostasis or otherwise neutralize the damaging consequences of the insult. One of the critical players in this process is GRP78 (glucose regulated protein of molecular weight 78), a calcium-binding protein that is primarily located in the ER lumen. It functions as a major chaperone during protein folding and also controls the activity of three major signaling pathways that originate from three different ER transmembrane proteins:

- IRE1α
- PERK
- ATF6

The lumenal domains of all of these proteins bind to the GRP78.

Inositol requiring enzyme 1a (IRE1α), which is conserved across eukaryotic species, contains a lumenal stress sensing domain and a cytosolic protein kinase domain. It is thought that IRE1α is activated by dimerization, which leads to trans-autophosphorylation and activation of a cytosolic endoribonuclease activity. To date, the only known substrate of the IRE1α endoribonuclease is X-box binding protein 1 (Xbp1) mRNA, from which a 26 base intron is removed by IRE1α. This splicing event alters the Xbp1 translational reading frame to fuse a C-terminal transactivation domain to the N-terminal DNA binding domain. The pancreatic ER eIF2α kinase (PERK) protein, which consists of a lumenal domain homologous to IRE1α and an unrelated cytosolic Ser/Thr kinase domain, similarly dimerizes or oligomerizes during ER stress. Its autophosphorylation directs PERK activity toward the subunit of the eukaryotic initiation factor 2 (eIF2) translation initiation complex. eIF2a phosphorylation inhibits delivery of the initiator methionyl-tRNAi to the ribosome and ultimately results in a general inhibition of protein translation. Finally, the activating transcription factor 6 (ATF6) protein is activated when ER stress liberates the molecule for transit from the ER to the Golgi, where regulated intramembrane proteolysis by site-1 protease and site-2 protease releases a cytosolic fragment that is a transcriptional coactivator. Based on the fact that IRE1α, PERK and ATF6 are freed from GRP78 during ER stress, GRP78 binding seems important in regulating, either directly or indirectly, activation of each arm of the UPR [24].

While GRP78 is difficult to detect in normal cells and generally requires their prior experimental exposure to ER-stress inducing agents, many tumor cell lines and primary clinical samples display permanently elevated levels of GRP78. This latter phenotype not only reflects these cells continuously ongoing effort to neutralize the potentially harmful effects of chronic stress within the tumor, but may also be an expression of permanent changes in cancer cell metabolism, such as Warburg effect. Unfortunately, because GRP78 also functions to suppress pro-apoptotic pathways, its elevated presence in tumor cells supports chemoresistance and thereby may worsen prognosis.

The protective effort of the ER-stress response does not have unlimited capacity. When ER stress becomes too severe, this system will turn on its pro-apoptotic program, which will trigger cell death despite the presence of high levels of GRP78. One of the decisive effectors of this switch is CHOP (CCAAT/enhancer binding protein homologous transcription factor). Increased levels of CHOP, a transcription factor, alters the transcriptional profile and facilitates a pro-apoptotic program that involves suppression of Bcl-2, stimulation of death receptor 5 (DR5), activation of caspases, and mitochondrial events that function to integrate and amplify the death pathway. In normal cells, CHOP is expressed at negligible levels. Similarly, tumor cells display insignificant amounts of CHOP, despite chronic ER stress, because elevated levels of GRP78 suppress those signaling pathways that are able to activate CHOP transcription (Fig. 9). In response to acutely increased ER stress, however, both normal and tumor cells stimulate CHOP expression, and the duration and amount of elevated CHOP levels are a decisive factor in determining the cell's fate. In case the protective components are able to regain control and subdue CHOP expression, the cell will survive. However, if severe ER stress persists, the pro-apoptotic program will attain dominance and will initiate cell death. Because of their relatively short-lived struggle for control, CHOP expression levels can be used as a convenient readout to reveal the acute phase of ER stress [25].
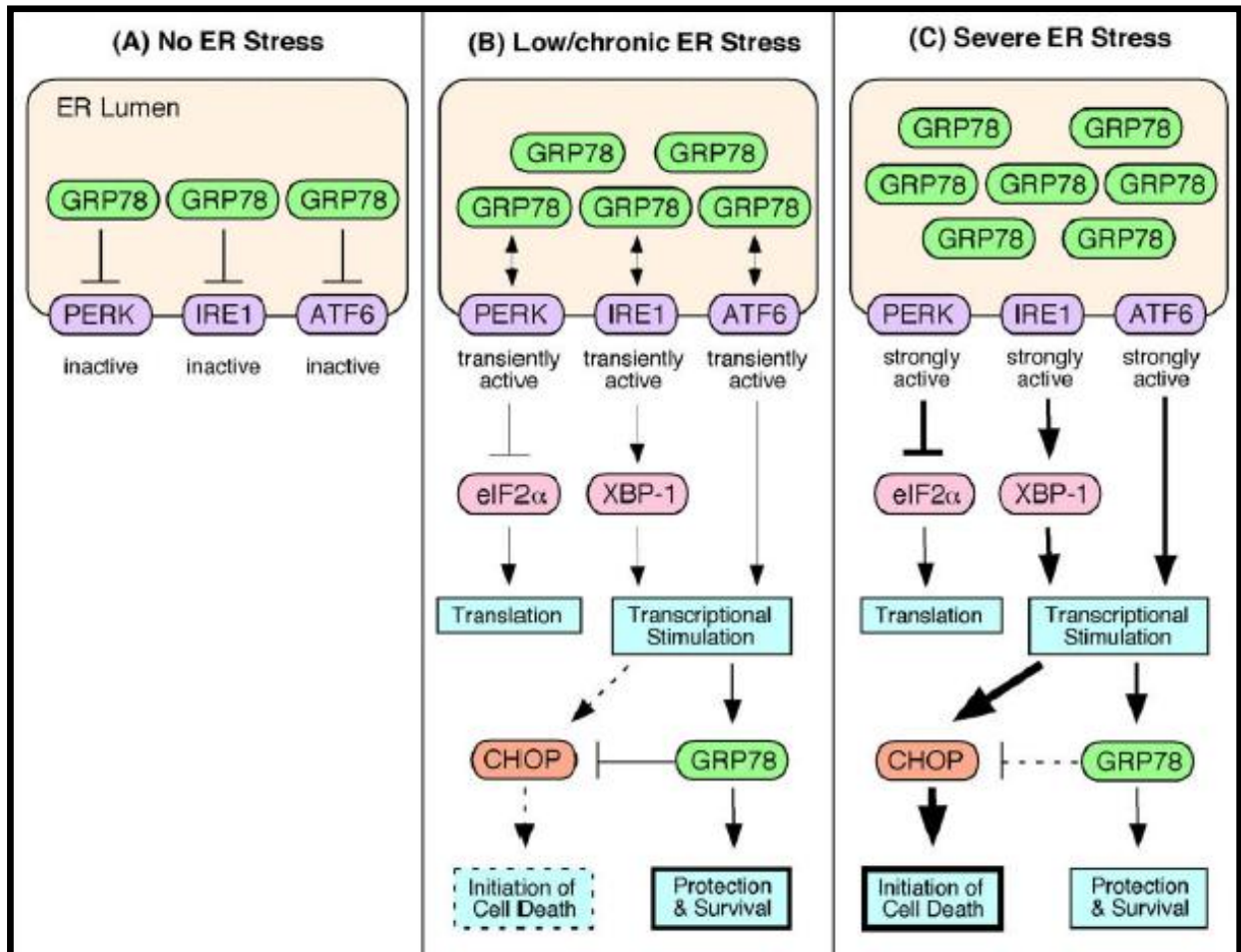
Figure 9: Differential ER stress levels, relating to normal cells (left panel), tumor cells or moderately stressed normal cells (middle panel), and moderately aggravated tumor cells or severely stressed normal cells (right panel).

Autophagy and ER-stress

The ER stress response is activated to protect the cells from different alterations affecting this organelle. However, when the intensity or duration of the ER damage cannot be restored by this response, ER stress can also lead to cell death. Likewise, autophagy can help cells to cope with ER stress (for instance contributing to the elimination of unfolded or aggregated proteins) or participate in the mechanism of ER stress induced cell death.

Evidence for a link between UPR and autophagy was obtained from ectopic expression of polyglutamine (polyQ) proteins. In these experiments, a dominant-

negative form of PERK or genetic substitution of Serine 51 of eIF2α by Ala (which prevents the phosphorylation of this protein) prevented polyQ protein [26] induced autophagy, strongly suggesting that PERKdependent eIF2α phosphorylation plays an important role in the activation of autophagy in response to the accumulation of unfolded proteins. On the other hand, eIF2α phosphorylation seems to be also important for autophagy as induced by other ER stress-related or unrelated stimuli [17, 27, 28]. It is important to bear in mind that PERK is not the only protein kinase regulating eIF2α phosphorylation, in fact PERK-eIF2α-dependent Atg12 upregulation is required for induction of autophagy in response to polyQ protein accumulation which suggests that controlling the expression of autophagy-related genes by eIF2α downstream targets could be one of the mechanisms connecting both events. In any case, further research is still necessary to clarify the precise mechanisms by which eIF2α phosphorylation regulates autophagy in response to different ER stress signals.

Activation of the IRE1 arm of the ER stress response has also been shown to regulate autophagy. Thus, treatment with tunicamycin or thapsigargin [29] or treatment with proteasome inhibitors [30] induced autophagy on an IRE1- dependent manner. The proautophagic actions of IRE1 seem to rely on the ability of this protein to interact with the cytosolic adaptor TRAF-2 and activate JNK [29]. Of interest, JNK has been proposed to regulate autophagy through Bcl-2 phosphorylation, which prevents this protein of interacting (and inhibiting) the essential autophagy regulator Beclin-1 [31, 32]. In addition, JNK has been shown to control Beclin-1 expression to regulate ceramide-induced autophagy. As discussed above, Beclin-1 is associated to the Vps34 and plays a very important role in the regulation of autophagy [33]. It is therefore conceivable that activation of the IRE1/TRAF2/JNK arm of ER stress may regulate autophagy through modulation of Beclin-1 function and expression. Intriguingly, it has been recently shown that XBP-1 ablation increases autophagy and protects from the toxicity induced by the aggregates of the enzyme superoxide dismutase 1 in a model of Amyotrophic lateral sclerosis [34]. These observations suggest that the XBP-1 may play a different role than TRAF2/JNK on the regulation of autophagy by the Ire1 arm of the UPR.

Purpose of the thesis

Purpose of the thesis

Pancreatic adenocarcinoma (PDAC) is one of the most aggressive and devastating human malignancies with a death-to-incidence ratio of 0.99 [3]. Although it represents only 2-3% of all cancers [4], pancreatic adenocarcinoma is the 4th cause of death by cancer after lung, prostate (breast in women), and colorectal cancers since 1970s.

Up to now, despite decades of efforts at elucidating molecular pathways involved in initiation and progression and at identifying effective therapies, the prognosis of pancreatic adenocarcinoma has not improved. At diagnosis, less than 20% of patients are candidates for surgery with curative intent [7].

Monotherapy with gemcitabine (GEM) has been the standard treatment during the last decade, although it has a response rate of less than 20% [8]. Then is very important to identify new molecules acting in synergy with the GEM.

Cannabinoids have been shown to have anti-proliferative, anti-metastatic, anti-angiogenic and pro-apoptotic effects in various cancer types (lung, glioma, thyroid, lymphoma, skin, pancreas, uterus, breast and prostate carcinoma) using both in vitro and in vivo models [14]. Since the cannabinoids are well tolerated by the body, their use in combination with GEM could be a new way to treat pancreatic adenocarcinoma.

The purpose of this thesis was to analyse the antiproliferative effects determined by addition of cannabinoids to GEM both in vitro and in vivo and to study some molecular mechanisms associated with them.

Materials and Methods

Materials and methods

Chemicals

Gemcitabine (2,2-difluorodeoxycytidine; GEM, Gemzar, Lilly) and ***N*-acetyl-ʟ-cysteine** (NAC) were freshly prepared in sterile water.

Arachidonoyl cyclopropamide (ACPA) was obtained from Cayman Chemicals (Inalco) already solubilised in ethanol and stored at −20 °C until use.

GW405833 hydrochloride [1-(2,3-dichlorobenzoyl)-2-methyl-3-(2-[1-morpholine] ethyl)-5-methoxyindole] was obtained from Sigma, solubilised in DMSO and stored at 4°C.

SR141716 (*N*-(piperidino-1-yl)-5-(4-chlorophenyl)-1-(2,4dichlorophenyl)-4-methyl-pyrazole-3-carboxamide; rimonabant; Acomplia®, Sanofi-Aventis) was kindly provided by Dr. Maurizio Bifulco (University of Naples, Italy), solubilised in DMSO and stored at −20°C until use.

E64d (Sigma) and **pepstatin A** (AppliChem) were solubilised in sterile water and ethanol, respectively, and stored at −20 °C until use.

MG-132 was obtained from Enzo Life Sciences, solubilised in DMSO and stored at 4°C.

BAY 11-7082 (E)-3-[(4-methylphenylsulfonyl]-2-propenenitrile was obtained from Enzo Life Sciences, solubilised in DMSO and stored at 4°C.

PDTC (Pyrrolidine dithiocarbamate) were obtained from Sigma, solubilised in water and stored at -80°C.

NAC (*N*-acetyl-L-cysteine) was obtained from Sigma, solubilised in ethanol and stored at -20°C.

Chloroquina diphosphate (CQ) [N^4-(7-chloro-4-quinolinyl)-N^1,N^1-dimethyl-1,4-pentanediamine] was obtained from Sigma, solubilised in water and stored at -20°C.

3-Methyladenine was obtained from Sigma and solubilised in RPMI. The powder was stored at -20°C.

Actinomycin D (ActD) was obtained from Sigma, solubilised in DMSO and stored at -80°C.

Cell culture

PaCa44, **PaCa3**, **Panc1**, **CFPAC1**, **T3M4**, and **MiaPaCa2** cell lines were grown in RPMI 1640 supplemented with:

    2 mM glutamine,

    10% FBS,

    50 µg/ml gentamicin sulfate (BioWhittaker).

Primary fibroblasts (PromoCell) were grown in DMEM supplemented with:

    2 mM glutamine,

    10% FBS,

    50 µg/ml gentamicin sulphate.

All cells were incubated at 37 °C with 5% CO_2.

Cell proliferation assay

Cells were plated in 96-well cell culture plates (5×10^3 cells/well) and treated with GEM and/or Cannabinoids. The compounds were added at the following range of concentrations:

Panc1, PaCa44 and PaCa3 cell lines:

- 1 nM → 1 μM for **GEM**,

- 80 nM → 80 μM for **SR1** and **GW405833**,

- 450 nM → 450 μM for **ACPA.**

T3M4, CFPAC and MiaPaCa2 cell lines:

- 0.2 nM → 200 nM for **GEM**,

- 100 nM → 100 μM for **SR1** and **GW405833**,

- 560 nM → 560 μM for **ACPA**

Cells were incubated for 48 h.

At the end of the treatments, cell proliferation was evaluated by Crystal Violet (Sigma) staining with the following protocol:

1. carefully remove culture medium from wells;

2. wash plate gently with PBS at room temperature;

3. carefully remove PBS and add crystal violet solution:

4. incubate 5 minutes at room temperature;

5. wash plate 2 times in tap water by immersion in a large beaker (be careful not to lift off cells and change tap water between washes);

6. drain upside down on paper towels, than add 100 μl of 1% SDS in PBS 1X to solubilize the stain;

7. agitate plate on orbital shaker until color is uniform with no areas of dense coloration in bottom of wells;

8. read absorbance photometrically (A_{595} nm) to determine cell viability.

Three independent experiments were performed for each assay condition.

Time-dependent analysis

Time-dependent growth curves of Panc1 and T3M4 cell lines treated with GEM/cannabinoids for 24 h. To maintain the molar ratios described above, Panc1 cells were treated with 25 nM GEM and/or 2 μM SR1, 2 μM GW, or 11.25 μM

ACPA, while <u>T3M4</u> cells were treated with 25 nM GEM and/or 12.5 μM SR1, 12.5 μM GW, or 70 μM ACPA.

The ratio on the Y axis was obtained by dividing the absorbance of untreated or treated cell lines by the mean absorbance of each cell line measured at time 0.

Drug combination studies

The combination index (CI) was calculated by the Chou–Talalay equation, which takes into account both the potency (IC_{50}) and the shape of the dose–effect curve, by using the CalcuSyn software (Biosoft, Cambridge, UK).

The general equation for the classic isobologram is given by

$$CI = (D)1/(Dx)1 + (D)2/(Dx)2 + [(D)1 \cdot (D)2]/[(Dx)1 \cdot (Dx)2]$$

where (Dx)1 and (Dx)2 in the denominators are the doses (or concentrations) for D1 (drug 1) and D2 (drug 2) alone that gives X% growth inhibition, whereas (D)1 and (D)2 in the numerators are the doses of drug 1 and drug 2 in combination that also inhibited X% cell viability (i.e., isoeffective).

The meaning of the CI value is:

- CI<1 ⟶ synergistic effect
- CI=1 ⟶ additive effect
- CI>1 ⟶ antagonistic effect
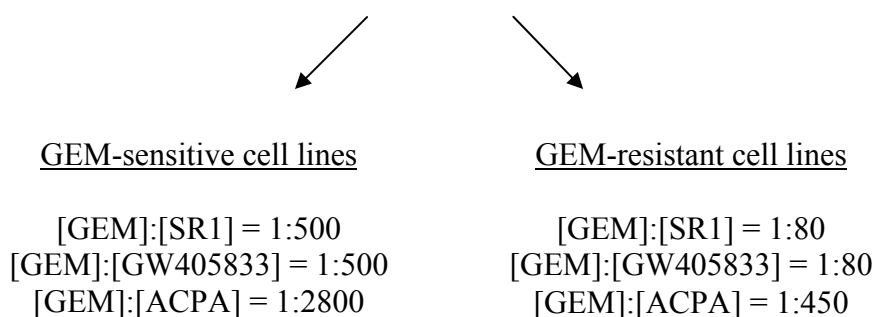
In accordance to manufacturer instructions we further differentiated the <u>synergistic effect</u> in:

- strong synergism (CI<0.3),
- synergism (0.3<CI<0.7),
- moderate synergism (0.7<CI<1).

CI/fractional effect curves represent the CI versus the fraction/percentage of cells affected/killed by drug combination. Indeed, the fractional effect is the % of growth inhibition corresponding to a given combination of the drugs. Dose reduction index (DRI) represents the measure of how much the dose of each drug in a synergistic combination may be reduced at a given effect level compared with the doses of each drug alone.

The linear correlation coefficient (*r*) of the median–effect plot is considered the first line of statistics to measure the conformity of the data with the mass–action law principle when the experimental measurement is assumed to be accurate.

Drug combination studies were performed using the following concentration ratios:

GEM-sensitive cell lines   GEM-resistant cell lines

[GEM]:[SR1] = 1:500   [GEM]:[SR1] = 1:80
[GEM]:[GW405833] = 1:500   [GEM]:[GW405833] = 1:80
[GEM]:[ACPA] = 1:2800   [GEM]:[ACPA] = 1:450

These molar ratios were calculated on the basis of GEM and cannabinoids IC_{50} mean values at 48 h. For GEM they correspond to 36 nM for the three GEM-sensitive cell lines tested and 220 nM for the three GEM-resistant cell lines tested.

The three cannabinoids were similarly effective in the six cell lines with IC_{50} mean values corresponding to 18 μM for SR1 and GW405833 and 100 μM for ACPA.

Analysis of reactive oxygen species (ROS)

The non-fluorescent diacetylated 2',7'-dichlorofluorescin (DCF-DA) probe, which becomes highly fluorescent on reaction with ROS, was used to evaluate intracellular ROS production.

Cells were plated in 96-well plates (5 x 10^3 cells/well) and the day after treated with the various compounds for 4 h and 16 h at the constant dose ratio:

<u>GEM</u>

     100-200-500 nM in Panc1 cells

     16-32-80 nM in T3M4 cells

<u>GW405833 and SR1</u>

     8-16-40 μM

<u>ACPA</u>

     40-90-225 μM

Then, cells were incubated with 10 μM DCF-DA (Sigma) for 15 min at 37 °C and then the DCF fluorescence was measured by using a multimode plate reader (Ex 485nm and Em 535nm).

RNA extraction with TRIzol, qPCR, RT-PCR and image analysis

1. <u>Cell lysis</u>:
   - add 1 ml of TRIzol at the cells,
   - homogenise by pipetting several times (mechanic lysis),
   - keep 5 min at RT for complete dissociation of nucleoprotein complexes.

2. <u>Phase separation</u>:
   - add 0.2 ml of chloroform to 1 ml of TRIzol,
   - shake for 15 sec,
   - incubate 2-5 min at RT,
   - spin 12000g, 15 min at 4°C.

3. <u>RNA precipitation</u>:
   - transfer aqueous upper phase into new tube,
   - add 0.5 ml of isopropanol to 1 ml of TRIzol,
   - incubate 10 min at RT,

- spin 12000 g, 10 min at 4ºC.

4. <u>RNA wash</u>:
    - remove supernatant,
    - wash pellet with 75% EtOH (1 ml EtOH to 1 ml of TRIzol),
    - spin 7500 g, 5 min at 4ºC.

5. <u>Redissolving of RNA</u>:
    - air-dry pellet for 5-10 min,
    - dissolve pellet in 50μl of H_2O RNase free,
    - incubate at 55-60 C° for 10 min
    - quantify the RNA.

For qPCR, the primers used were:

CB1 For   5'-GAGAGGTGCCAAGGGAGCTT-3'

CB1 Rev   5'-GGTGCGGAAGGTGGTATCTG-3';

CB2 For   5'-CACAGCCTCTGTGGGTAGCC-3'

CB2 Rev   5'-ACGGGTGAGCAGAGCTTTGT-3';

Grp78 For   5'-GACGGGCAAAGATGTCAGGAA-3'

Grp78 Rev   5'-TCATAGTAGACCGGAACAGATCCA-3';

CHOP For   5'-GCAGCCCATGAAGGAGAAAG-3'

CHOP Rev   5'-CGGTCGATTTCCTGCTTGAG-3',

GAPDH For 5'-TGTGTCCGTCGTGGATCTGA-3'

GAPDH Rev 5'-R-GATGCCTGCTTCACCACCTT-3'.

The following cycling conditions were used: 95 °C for 10 min, 40 cycles at 95 °C for 15 s, 60 °C for 1 min and 72 °C for 30 s. The average of cycle threshold (CT) of each triplicate was analyzed according to the $2^{(-\Delta\Delta Ct)}$ method.

For RT-PCR, one tenth of the cDNA was used as a template for PCR amplification using the following primers and cycling conditions:

β-actin For   5′-ACCAACTGGGACGACATGGAGAA-3′

β-actin Rev   5′-GTGGTGGTGAAGCTGTAGCC-3′,

25 cycles of 94 °C for 60 s, 55 °C for 60 s and 72 °C for 60s;

XBP-1 For   5′-CCTTGTAGTTGAGAACCAGG-3′

XBP-1 Rev   5′-GGGGCTTGGTATATATGTGG-3′,

40 cycles of 93 °C for 60 s, 55 °C for 60 s and 72 °C for 60 s.

PCR products were separated by electrophoresis through ethidium bromide-stained 3.5% agarose gel and visualized by ultraviolet light. To quantify XBP-1 splicing, XBP-1(S) bands were scanned as digital peaks and the areas of the peaks were calculated using the public domain NIH Image software (http://rsb.info.nih.gov/nihimage/), normalized with β-actin mRNA expression, and reported as fold induction relative to controls.

For actinomycin D experiments, 2.5 x 10^5 Panc1 cells were seeded in 60 mm plates and incubated overnight. Cells were pre-treated with 0.5 μg/μl Actinomycin D for 1 hour, then 2 μM GEM was added and the treatments prolonged up to 16 hours. Total RNA extraction and real-time PCR were performed as above described.

Apoptosis

The percentage of apoptotic cells was evaluated by staining 3×10^5 cells with annexin V-FITC (Bender Med System) and 5 µg/ml propidium iodide in binding buffer for 10 min at room temperature in the dark.

The samples were analyzed by flow cytometry (FACScalibur, Becton-Dickinson) to determine the percentage of cells displaying:

Early apoptosis	Late apoptosis
Annexin V^+ / propidium iodide⁻ staining	Annexin V^+ / propidium iodide⁺ staining
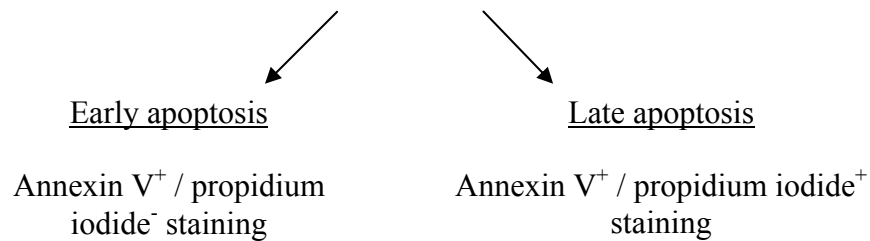
Cells were treated with 200 nM GEM and/or 16 µM SR1, 90 µM ACPA, or 16 µM GW405833 for 48 h.

BINDING BUFFER:

       10 mM HEPES/NaOH (pH 7.4),

       140 mM NaOH,

       2.5 mM $CaCl_2$.

Cell cycle analysis

Cell cycle distribution was analyzed using propidium iodide (PI)-stained cells.

Cells were:

1. washed with PBS,
2. incubated with:
   - 0.1% sodium citrate dihydrate,
   - 0.1% Triton X-100, 200 µg/ml RNase A,
   - 50 µg/ml propidium iodide (Roche Molecular Biochemicals)
3. analyzed using a flow cytometer (FACScalibur, Becton Dickinson).

The percentage of cells in the various stages of the cell cycle was determined using the ModFitLT software.

Cells were treated with 200 nM GEM and/or 16 μM SR1, 90 μM ACPA, or 16 μM GW405833 for 48 h.

Immunoblot analysis

Cells were plated in cell culture plates (1.2×10^6 cells/plate). Western blot analysis of LC3 was performed using total protein extracts from Panc1 cells treated with 500 nM GEM and/or 40 μM GW, 225 μM ACPA SR1, or 40 μM SR1 for 24 h. The concentration of NAC (N-acetyl-L-cysteine) was 10 mM.

1. At the end of the treatments cells were:
   - collected,
   - washed in phosphate-buffered saline,
   - resuspended in RIPA buffer pH 8,
   - kept for 30 min on ice.
2. The lysate was centrifuged at 14,000×g for 10 min at 4 °C and the supernatant was used for Western blot.
3. Protein concentration was measured with the Bradford protein assay reagent (Pierce) using bovine serum albumin as a standard. Fifty (LC3-II) or thirty (Grp78) micrograms of protein extracts were electrophoresed through a 15% SDS-polyacrylamide gel and electro-blotted onto PVDF membranes (Millipore, Bedford, MA).
4. Membranes were then incubated for 2 h at room temperature with blocking solution and probed overnight at 4 °C with the appropriate primary antibody [1:1000 in blocking solution of LC3B (Cell Signaling) or α-tubulin (Oncogene) antibodies].
5. Horseradish peroxidase conjugated IgG (1:2000 in blocking solution, Upstate Biotechnology) was used to detect specific proteins.

6. Immunodetection was carried out using chemiluminescent substrates (Amersham Pharmacia Biotech) and recorded using a HyperfilmECL (Amersham Pharmacia Biotech).

To quantify the autophagy, LC3 bands were scanned as digital peaks and the areas of the peaks relative to LC3-II were calculated in arbitrary units using the public domain NIH Image software (http://rsb.info.nih.gov/nihimage/) and reported as fold induction relative to controls. α-tubulin was used as a normalizing factor.

The choice to consider only the amount of LC3-II for autophagy analysis, rather than LC3-II/LC3-I ratio, was derived from the evaluation performed by Mizushima et Yoshimori.

RIPA buffer pH8

150 mM NaCl; pH 8,

50 mM Tris-HCl;

1% NP-40;

0.5% Na-Doc;

0.1% SDS;

1 mM PMSF;

1 mM Na_3VO_4;

1 mM NaF;

2.5 mM EDTA;

1× protease inhibitor cocktail (Roche)

Western blot solution:

RUNNING BUFFER:

25 mM Tris-HCl, pH 8.3

190 mM Glycine

SDS 0.1%

BLOCKING SOLUTION:

5% low-fat milk in TBST 1X

TBST:

100 mM Tris, pH 7.5

NaCl 0.9%

Tween 20 0.1%

TRANSFER BUFFER:

25 mM Tris-HCl, pH 8.3

190 mM Glycine

150 ml MetOH

SAMPLE BUFFER 4X:

200 mM Tris-HCl, pH 6.8

SDS 8%

Glycerol 40%

Bromophenol blue 0.4%

Labeling of autophagic vacuoles with monodansylcadaverine (MDC)

To quantify the induction of the autophagic process in Panc-1 cells treated with the various compounds as indicated in the legend, MDC staining was performed as previously described [35]. Following the treatments, cells were incubated with 50 μM MDC in PBS at 37°C for 15 min. After incubation, cells were washed with PBS, trypsinized and immediately analyzed by flow cytometry. All fluorescences were analyzed with a FACScalibur flow cytometer (Becton Dickinson, California). The fluorescent emissions were collected through a 530 nm band pass filter (FL1 channel). At least 10,000 events were acquired in log mode. For the quantitative evaluation of MDC, CellQuest software (Becton Dickinson) was used to calculate

mean fluorescence intensities (MFIs). The MFIs were calculated by the formula (MFItreated/MFIcontrol), where MFItreated is the fluorescence intensity of cells treated with the various compounds and MFIcontrol is the fluorescence intensity of untreated and unstained cells.

Quantification of acidic vescicle organelles with acridine orange

In acridine orange-stained cells, the cytoplasm and nucleus are bright green and dim red, whereas acidic compartments are bright red. The intensity of the red fluorescence is proportional to the degree of acidity. Following the treatments as specified in the legend, cells were incubated with acridine orange solution (1 μg/ml) at 37˚C; after 15 min in drug-free medium at 37˚C, they were washed with PBS, immediately stained with 1 μg/ml of acridine orange for 15 min, and observed with a Nikon Eclipse TE300 Inverted microscope.

Then, cells were trypsinized and analyzed by flow cytometry using FACScan cytometer and CellQuest software, as previously described.

In vivo studies

On the basis of our previous experience, we did not use Panc1 cells for in vivo studies because of their low growth rate in nude mice. Thus, we chose PaCa44 cells for their very similar behaviour to Panc1 cells after GEM/cannabinoid treatments in vitro. PaCa44 cells (2×10^6 cells/mice) were s.c. injected into female nude mice (4 weeks of age, Harlan laboratories). One week after cell inoculation, 5 randomized animals for each experimental group received solution vehicle (PBS), 25 mg/Kg GEM, or/and 0.28 mg/Kg SR1 by intraperitoneal injection biweekly for 4 weeks. Although drug molar ratios are different to that used in our in vitro studies, drug doses were chosen on the basis of their respective clinical use following US Food and Drug Administration directives. Tumour volume and body mass were biweekly recorded for each animal. Animals were sacrificed at the end of the 4-week study period and

the tumours were resected and weighted. The animal studies were approved by the Verona University Review Board.

Statistical analysis

ANOVA (post hoc Bonferroni) analysis was performed by GraphPad Prism version 5. *P* values less than 0.05 or 0.01 were indicated as ** or ***, respectively.

Results

Results

The cannabinoids GW, ACPA, and SR1 inhibit pancreatic adenocarcinoma cell proliferation

The inhibition of cell proliferation by GW (GW405833 hydrochloride), ACPA (arachidonoyl cyclopropamide), and SR1 (SR141716) was examined by measuring the growth of six pancreatic adenocarcinoma cell lines at 48 hours following treatment with increasing concentrations of cannabinoids. All cell lines analyzed showed a strong inhibition of growth (Fig. 10), with an average IC_{50} value corresponding to 18 μM for GW and SR1 and
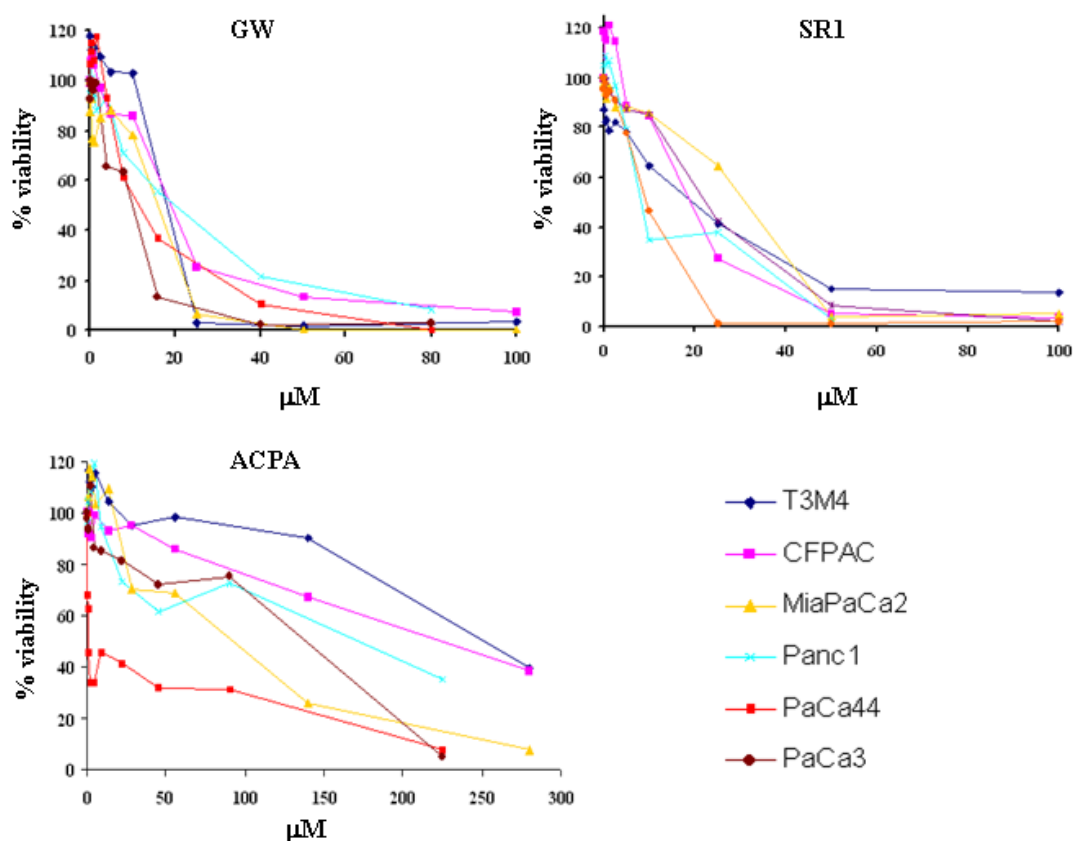
Figure 10: The cannabinoids inhibit the proliferation of six cell lines of pancreatic adenocarcinoma. The cells were treated with increasing concentrations of GW, SR1, and ACPA for 48 hours and the cell proliferation was measured using crystal violet. The values presented are the mean of three independent experiments.

Cell proliferation assay after GEM/cannabinoid treatment

To investigate if the synthetic cannabinoids SR1, ACPA, and GW were able to enhance cell growth inhibition induced by GEM, we performed dose-dependent analyses of cell viability on six pancreatic adenocarcinoma cell lines.

As established in previous analyses, the IC_{50} at 48 hours of treatment with GEM is different for the six tumor cell lines studied:

- PaCa44, Panc1 and PaCa3 are more <u>resistant</u> to GEM treatment and have an average IC_{50} of 220 nM (R lines)

- MiaPaCa2, T3M4 and CFPAC1 are more <u>sensitive</u> to GEM treatment and have an average IC_{50} of 36 nM (S lines) [12].

In the combination studies with GEM/cannabinoids, we chose two different molar ratios for the two groups of cell lines, R and S, based on the mean IC_{50} of cannabinoids and GEM. The molar ratio was:

- for the <u>resistant</u> cell lines
  - (1:80) for GEM/GW and GEM/SR1
  - (1:450) for GEM/ACPA
- for the <u>sensitive</u> cell lines
  - (1: 500) for GEM/GW and GEM/SR1
  - (1:2800) for GEM/ACPA

Figure 11 shows the cell viability of Panc1 and T3M4 cell lines after 48 h treatment with increasing concentrations of single or combined drugs. At the higher concentrations, cannabinoids, but not GEM, were generally able to totally inhibit cell viability. In the combined treatments, proliferation of Panc1 cells was further inhibited in almost all conditions, while that of T3M4 cells was only sporadically reduced. Similar results were obtained with the other pancreatic adenocarcinoma cell lines tested in this study.

The antiproliferative effect of the combination GEM/cannabinoids, as compared to single-drug treatments, was stronger in GEM-resistant than in GEM-sensitive cell lines. By inverting the molar ratios of the compounds between the two groups of cell lines, no significant alteration of the results was observed, indicating that the differential behaviour was not due to the specific experimental condition tested.
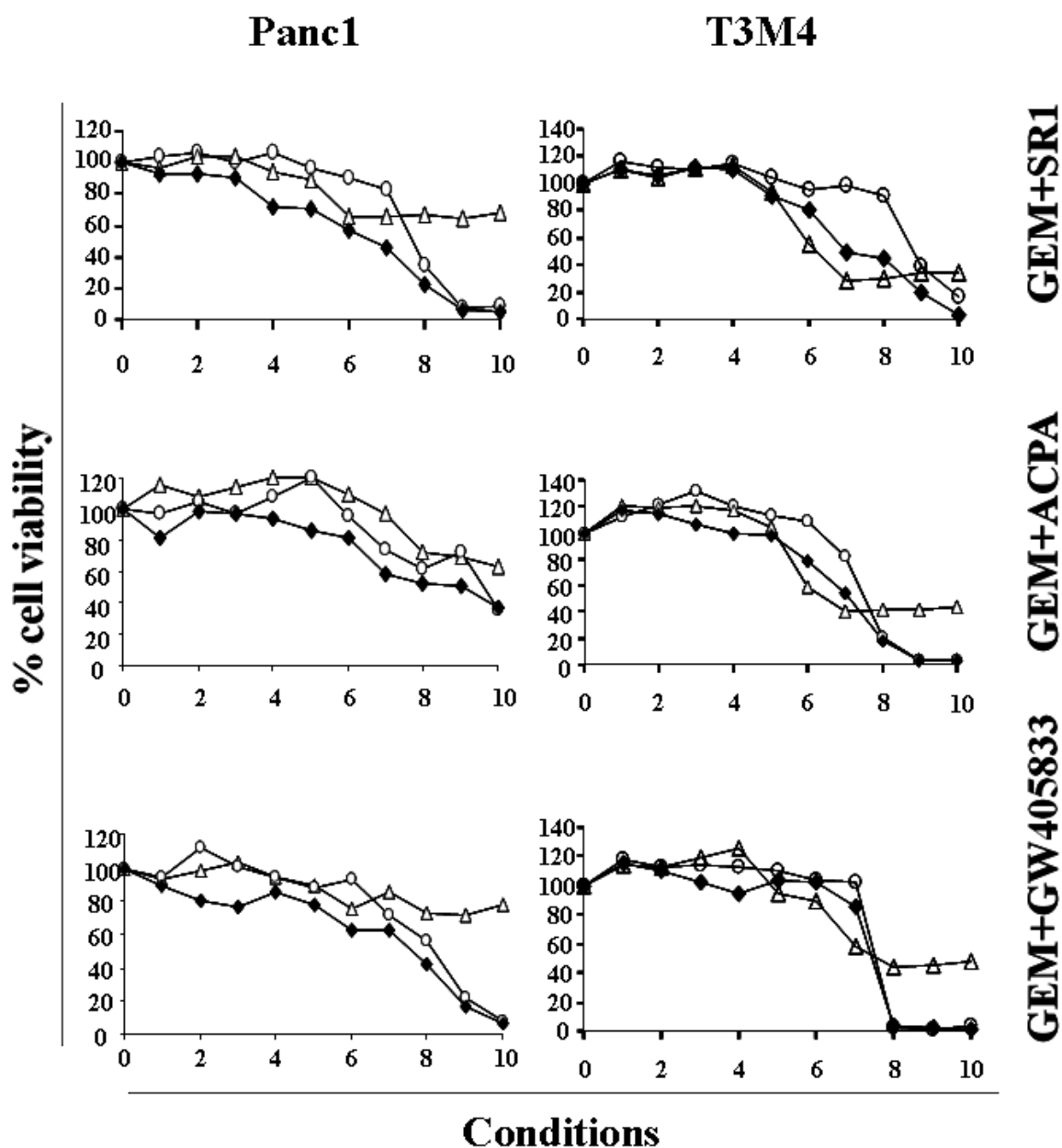
Figure 11: Effect of increasing concentrations of GEM and/or the cannabinoids SR1, ACPA, or GW on Panc1 and T3M4 pancreatic adenocarcinoma cell growth. The compounds were added at the following range of concentrations: 1 nM → 1 μM for GEM, 80 nM → 80 μM for SR1 and GW405833, 450 nM → 450 μM for ACPA in Panc1 cell line; 0.2 nM → 200 nM for GEM, 100 nM → 100 μM for SR1 and GW405833, 560 nM → 560 μM for ACPA in T3M4. GEM concentration for each condition corresponds to: 1, 2, 5, 10, 20, 50, 100, 200, 500 nM, and 1μM for Panc1 cells and 0.2, 0.5, 1, 2, 5, 10, 20, 50, 100, and 200 nM for T3M4 cells. Cells were incubated for 48 h. Empty triangle, empty circle, and black rhombus correspond to GEM, cannabinoids, and combined treatments, respectively. Values are the means of triplicate wells from three independent experiments.

To examine the sensitivity of normal cells to GEM/cannabinoid treatments, we performed cell viability analyses on human primary fibroblasts. Drug combinations were not able to increase the cytotoxic effect of GEM or cannabinoids alone, both with the drug molar ratios used for GEM-resistant and GEM-sensitive cell lines (Figure 12).
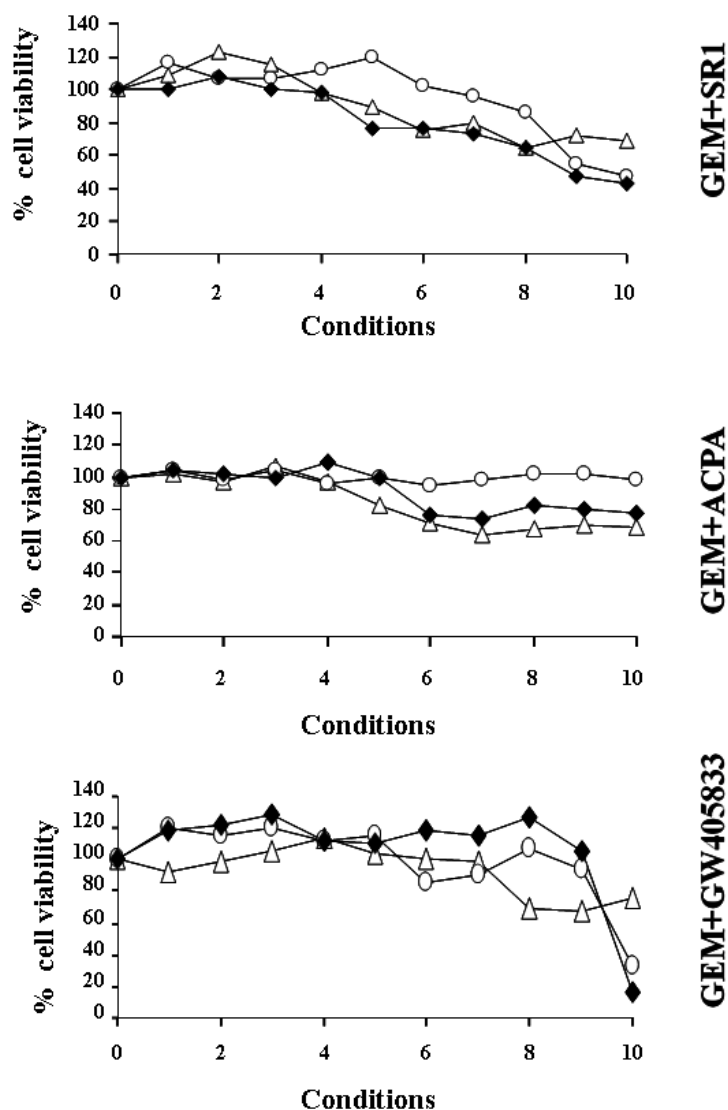
Figure 12: Effect of increasing concentrations of GEM and/or the cannabinoids SR1, ACPA, or GW on normal fibroblast cell growth. The compounds were added at the following range of concentrations: 1 nM → 1 µM for GEM, 80 nM → 80 µM for SR1 and GW405833, 450 nM → 450 µM for ACPA. GEM concentration for each condition corresponds to: 1, 2, 5, 10, 20, 50, 100, 200, 500 nM, and 1µM. Cells were incubated for 48 h. Empty triangle, empty circle, and black rhombus correspond to GEM, cannabinoids, and combined treatments, respectively. Values are the means of triplicate samples from three independent experiments.

The combined treatment GEM/cannabinoid synergistically inhibits pancreatic adenocarcinoma cell proliferation

To evaluate whether cell growth inhibition by GEM/cannabinoids was synergistic, we analyzed the cell viability curves by using the dedicated software CalcuSyn. Figure 13 reports the isobolograms of the combination index (CI) values versus the fraction (0→1) of cells killed by the different drug combinations in the GEM-resistant cell lines. All combinations gave rise to a significant synergistic reduction of cell viability.

GEM+SR1
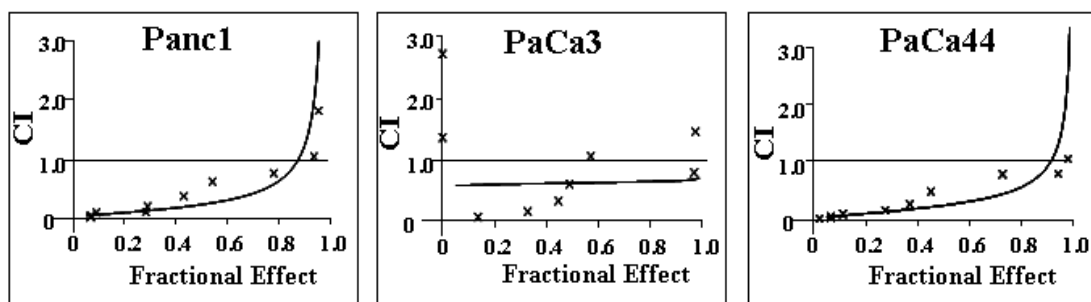
GEM+ACPA
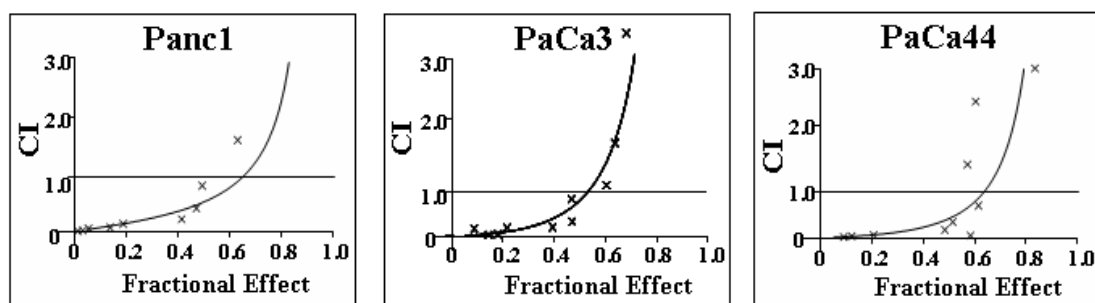
GEM+GW405833
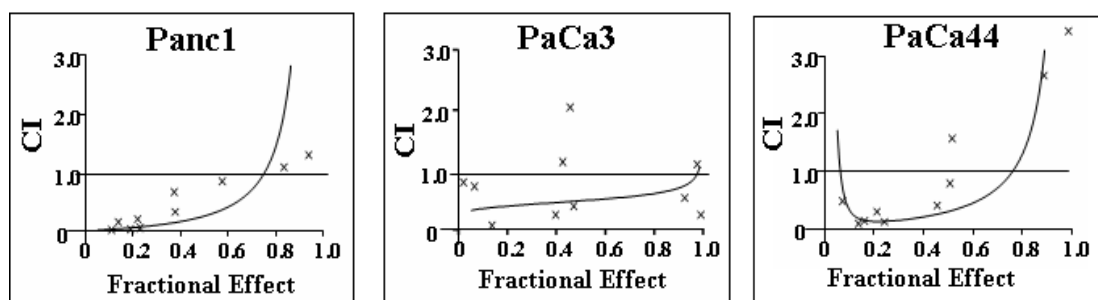
Figure 13: Combination index (CI)/fractional effect curves of the antiproliferative effect after 48 h treatment of Panc1 (see fig. 1), PaCa3, and PaCa44 cell lines with increasing concentrations of GEM/cannabinoids. The values on the X-axis correspond to the fraction of growth inhibition by increasing concentrations of drug combinations.

Figures 14 and 15 report the percentages of the <u>C</u>ombination <u>I</u>ndex (CI) values encompassed between 1 and 0.3 (synergism) or lower than 0.3 (strong synergism) for all combinations. Although GEM resistant cell lines showed similar percentages of overall synergism to GEM sensitive cell lines, it is worth to note that the former cell lines show a significant higher level of strong synergism (CI<0.3) compared to the latter cell lines, as reported in figure 14. Instead, GEM/cannabinoids did not determine any synergisms in normal fibroblasts.
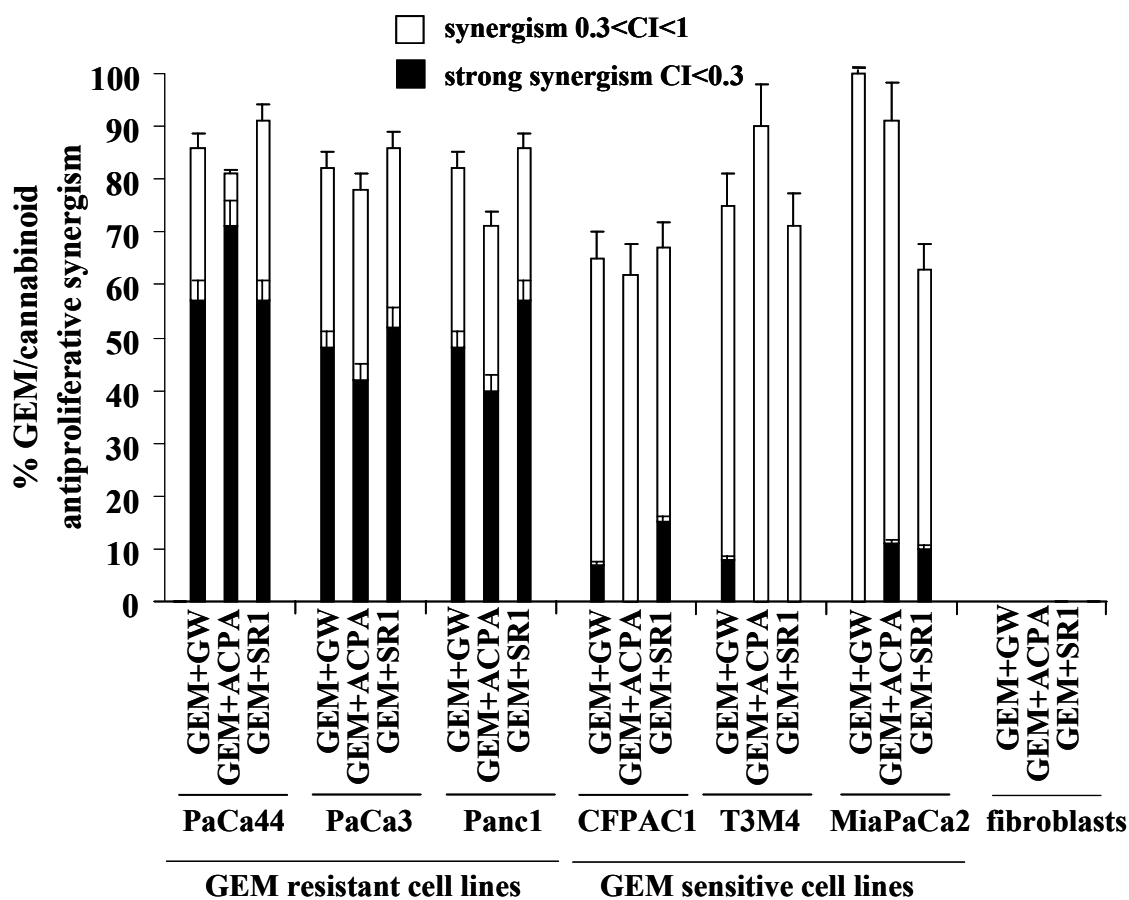
Figure 14: Percentages of GEM/cannabinoid antiproliferative synergism in six pancreatic adenocarcinoma cell lines and normal fibroblasts. The percentage values were obtained by analyzing CI/effect curves. Statistical analysis: $p < 0.001$, % CI<1 in all cancer cell lines versus normal fibroblasts.
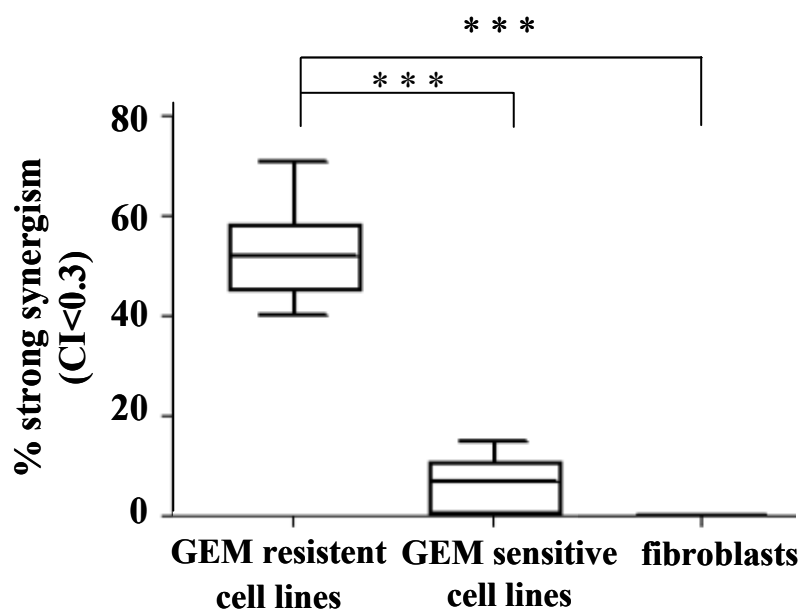
Figure 15: GEM/cannabinoids determined a significant antiproliferative strong-synergism (CI<0.3) in GEM-resistant as compared to GEM-sensitive cell lines and normal fibroblasts. The percentage values were obtained by analyzing CI/effect curves

As shown in figure 16, a good correlation exists between the GEM IC_{50} values of the six cell lines and the synergism/strong synergism (CI<0.7) obtained with all GEM/cannabinoid combinations.
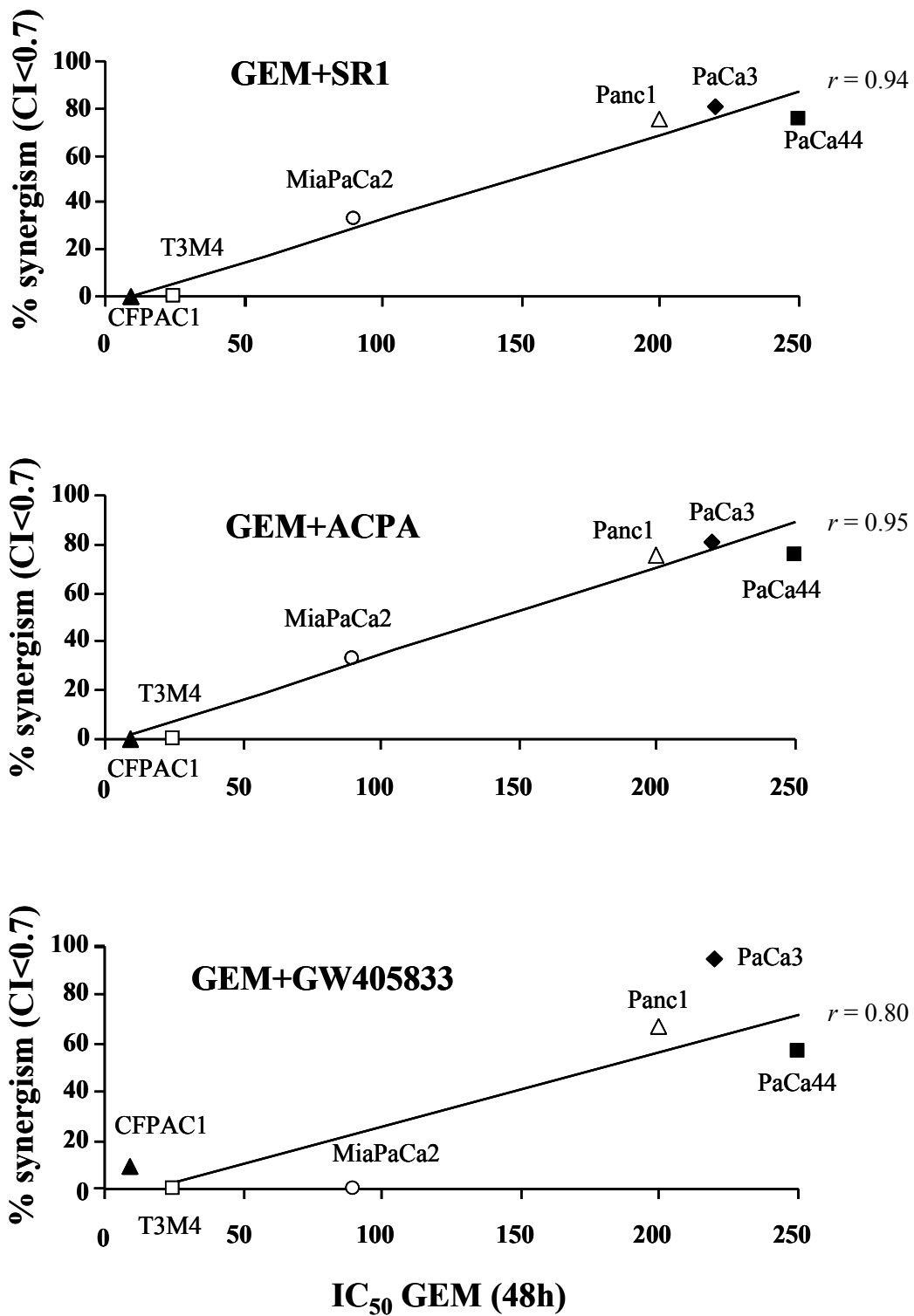
Figure 16: Correlation between GEM resistance and GEM/cannabinoid antiproliferative synergism. The CI/effect curves were analysed to determine the CI values for each 0.05 fraction of the effect. The mean percentage values of synergism (CI<0.7) were plotted versus the GEM IC50 at 48 h for each pancreatic adenocarcinoma cell line.

To analyze the trend of the inhibitory effect over the time, we performed a time-dependent analysis of the antiproliferative activity following a 24 h single-step treatment with GEM and/or cannabinoids. Figure 17 shows that starting from the fourth day the combined, but not the single treatments, were able to significantly inhibit Panc1 cell proliferation, with a growth rate inhibition at the sixth day in treated versus untreated cells of 48%, 36%, and 57% for GEM/GW, GEM/ACPA, and GEM/SR1, respectively, but not T3M4 cell proliferation.
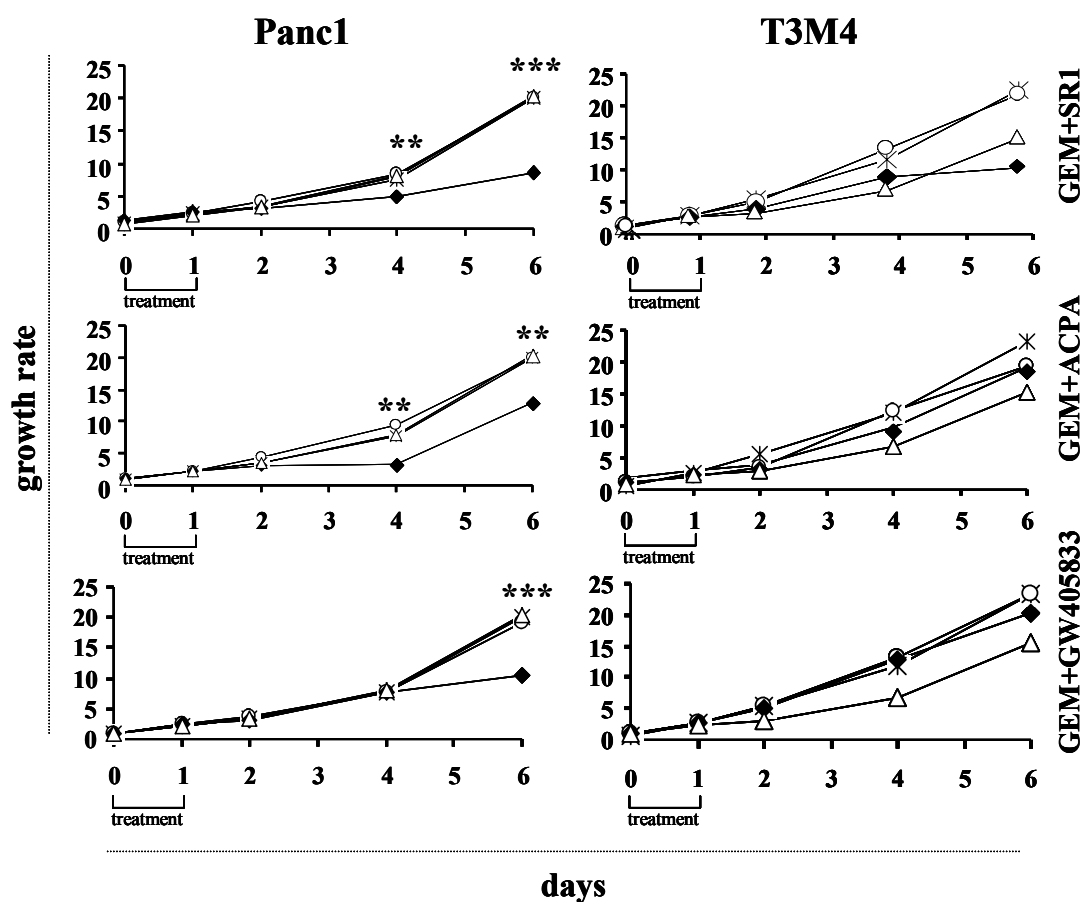
Figure 17: Effect of GEM and/or GW, ACPA, or SR1 on growth of pancreatic adenocarcinoma Panc1 and T3M4 cells. The cells were seeded in 96-well plates and incubated overnight. The compounds were added at the following concentrations for 24 h: 25 nM GEM and/or 2 μM SR1, 2 μM GW, or 11.25 μM ACPA. The growth ratio on the Y-axis was obtained by dividing the absorbance of untreated or treated cell lines by the mean absorbance of each cell line measured at time 0. Star, empty triangle, empty circle, and black rhombus correspond to control, GEM, cannabinoids, and combined treatments, respectively. Values are the means of triplicate samples from three independent experiments (±SD). The statistical analysis reported was performed for each combined treatment versus control.

58

GEM/cannabinoids enhance intracellular ROS production

Previously published data of our group have reported that GEM is able to induce ROS and that an inverse correlation exists between resistance to GEM and constitutive ROS levels in pancreatic adenocarcinoma cells [11]. To verify whether SR1, ACPA, or GW further enhanced ROS production by GEM, we measured ROS levels in Panc1 and T3M4 cells treated with increasing doses of the drugs. Figure 18 shows that 4 h GEM/cannabinoid treatments determined a significant enhancement of ROS relative to single treatments in Panc1, but not in T3M4 cells. Similar results were obtained after 16 h or by inverting the molar ratios of the compounds between the two cell lines.
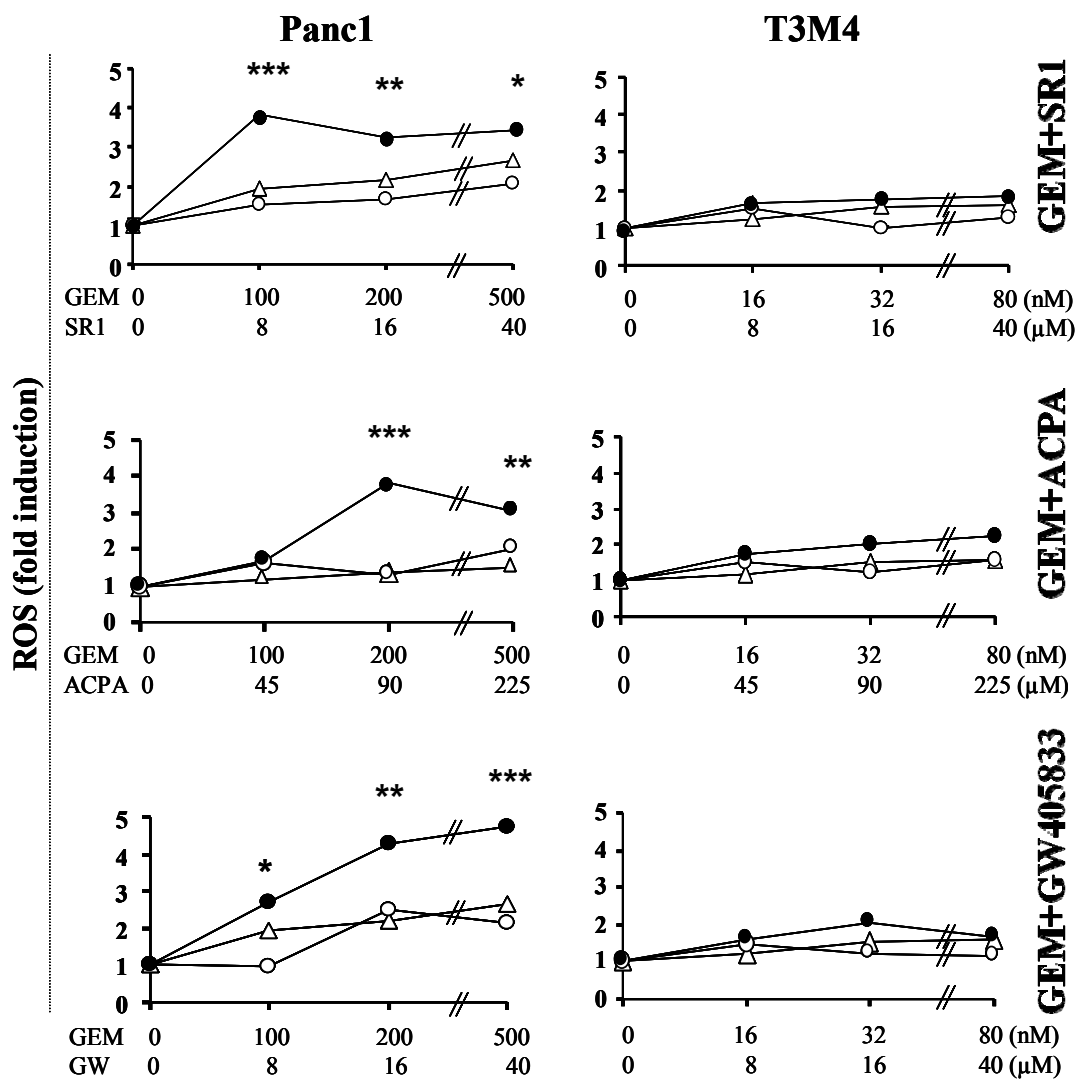
Figure 18: Effect of GEM and/or cannabinoids on intracellular ROS production in Panc1 and T3M4 cell lines. Cells were treated with increasing concentrations of the compounds for 4 h at the constant dose ratios. The 2′,7′-dichlorofluorescin (DCF) fluorescence intensity, corresponding to the level of ROS production, was measured by a multimode plate reader. Empty triangle, empty circle, and black circle correspond to GEM, cannabinoids, and combined treatments, respectively. Values are the means of triplicate samples from three independent experiments. The statistical analysis was performed for each combined treatment versus single treatments.

To analyze the functional role of ROS enhancement in the synergistic antiproliferative effect by combined treatments, we used a non-toxic concentration (10 mM) of the antioxidant compound N-acetyl-$_L$-cysteine (NAC) that was able to completely abolish ROS induction by GEM/cannabinoids. Figure 19 and data analysis by the CalcuSyn software reveal that NAC addition abolished the enhanced cell growth inhibition and the antiproliferative synergism by all three combined treatments in Panc1 cells.
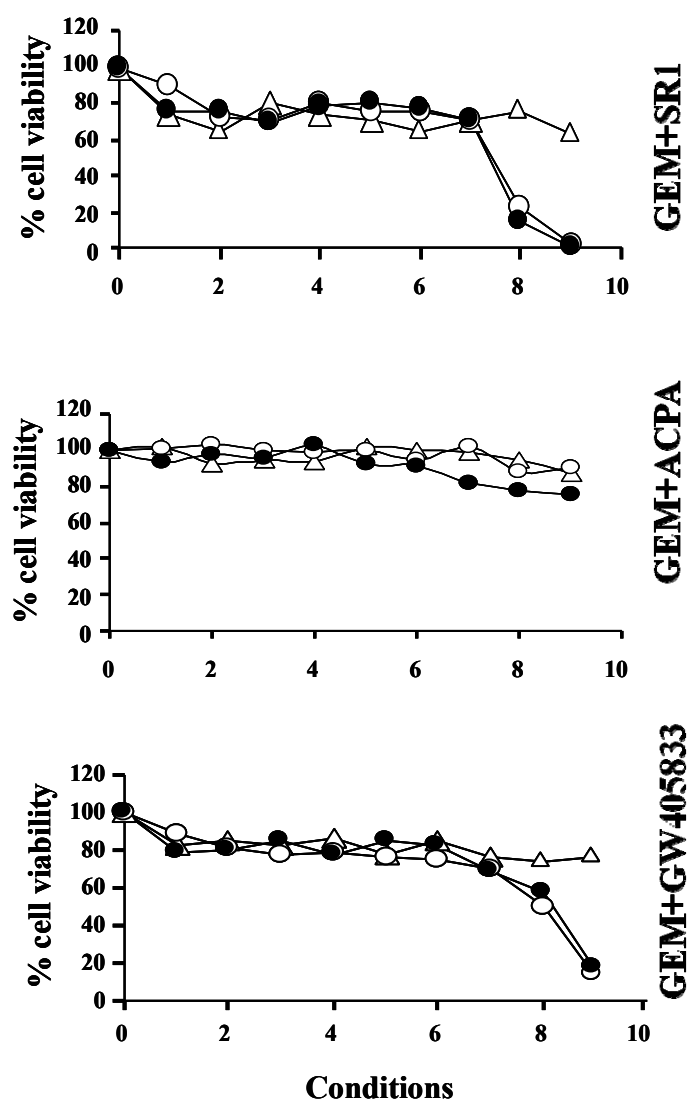

Figure 19: Effect of increasing concentrations of GEM and/or cannabinoid compounds SR1, ACPA, or GW405833 on Panc1 cells in the presence of 10 mM NAC. Cells were seeded in 96-well plates and incubated overnight. The day after cells were pre-treated with 10 mM NAC for 1 h and then treated for 48 h with the various compounds at the following range of concentrations: 1 nM → 0.5 μM for GEM, 80 nM → 40 μM for SR1 and GW405833, 450 nM → 225 μM for ACPA. Each condition corresponds to a GEM concentration of: 1, 2, 5, 10, 20, 50, 100, 200, and 500 nM. Empty triangle, empty circle, and black circle correspond to GEM, cannabinoids, and combined treatments, respectively. Values are the means of triplicate samples from three independent experiments.

61

GEM induces cannabinoid receptor expression by NF-κB mediated mechanism

Since it was described that cannabinoid receptor overexpression was a mechanism able to potentiate cannabinoid effect [36], we investigated whether GEM induces CB1 and CB2 receptor expression in Panc1 cells. As shown in figure 20, GEM determined a 4.4-fold induction of CB1 mRNA at 24 h and a 7.7-fold induction of CB2 mRNA at 16 h.
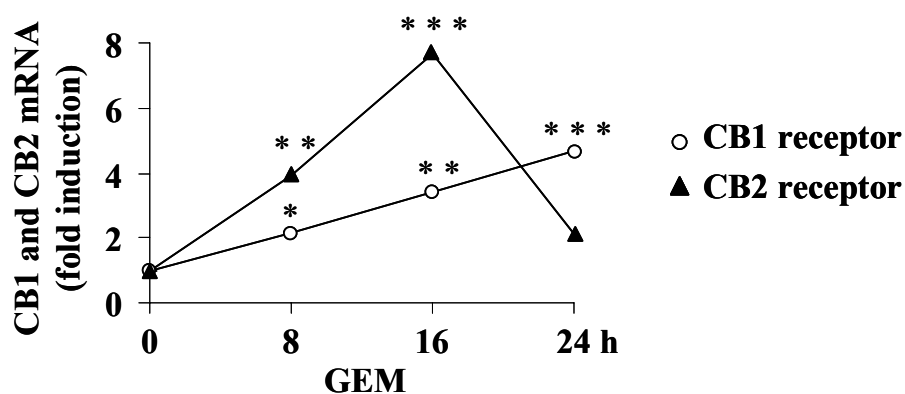

Figure 20: Analysis of CB1 and CB2 cannabinoid receptor gene induction by GEM in Panc1 cells. qPCR assay was performed on cells treated with 2 μM GEM at the indicated time points. Values are the means of three independent experiments. The statistical analysis reported was relative to GEM treatment versus control.

CB mRNAs induction by GEM was transcriptionally regulated, as indicated by their complete inhibition following Actinomycin D treatment (Figure 21) and was reversed by three NF-κB inhibitors (BAY, PDTC, and MG132), but not by the free radical scavenger NAC (Figure 22).
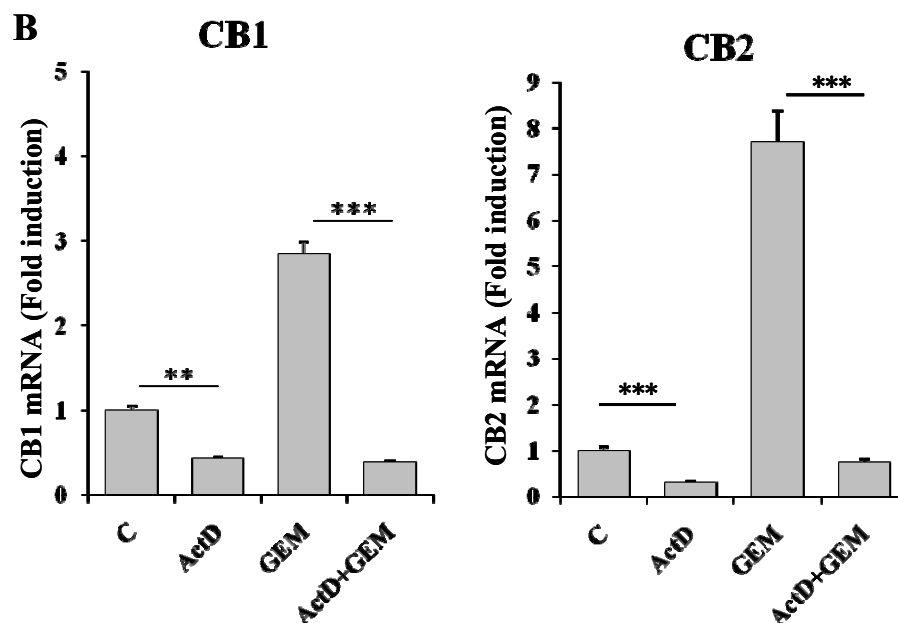
Figure 21: Panc1 cells were seeded in 60 mm plates and incubated overnight. Cells were pre-treated with 0.5 μg/μl Actinomycin D for 1 hour, then 2 μM GEM was added and the treatments prolonged up to 16 hours. Total RNA extraction and real-time PCR were performed as described in Materials and Methods. Values are the means of triplicate samples from four independent experiments (±SD). Statistical analysis: *** p<0.001, ** p<0.01.
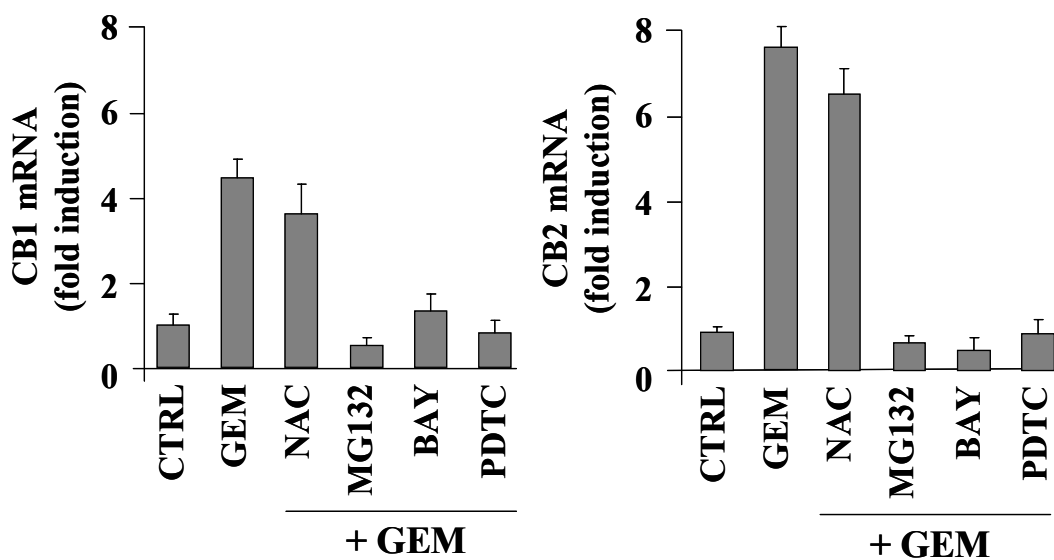

Figure 22: qPCR analysis of CB1 and CB2 gene induction by 2 μM GEM alone or in combination with 10 mM NAC, 100 μM MG132, 10 μM BAY, or 100 μM PDTC which were added 1 h before. CB1 and CB2 gene expression was analyzed at 24 h and 16 h, respectively. Values are the means of triplicate samples from three independent experiments (±SD). p<0.001 control versus GEM or GEM+NAC; p<0.001 GEM versus GEM+MG132, GEM+BAY, or GEM+PDTC. The same significance was observed for both CB1 and CB2.

IL-1, a known NF-κB inducer, was able to stimulate CB1 and CB2 induction and both GEM and IL-1-mediated cannabinoid receptor enhancement was dramatically increased by the addition of the histone deacetylase inhibitor TSA. Furthermore, the addition of the NF-κB inhibitor MG132 completely reversed these effects (figure 23).
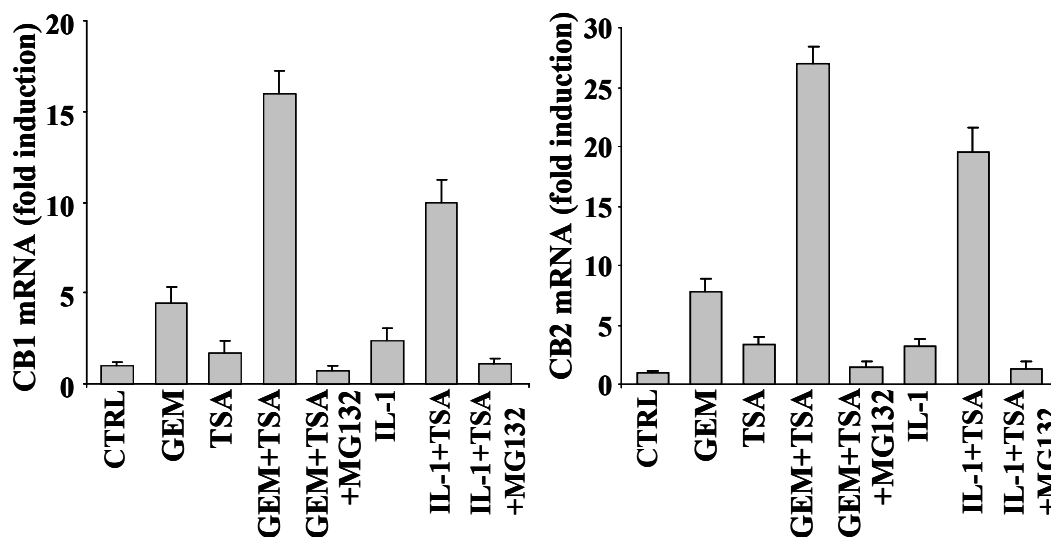

Figure 23: qPCR analysis of CB1 and CB2 gene induction by the indicated treatments using 2 μM GEM, 0.2 μM TSA, 100 μM MG132, and 10 μg/ml IL-1. CB1 and CB2 gene expression was analyzed at 24 h and 16 h, respectively. Values are the means of triplicate samples from three independent experiments (±SD). p<0.001 GEM versus GEM+TSA or GEM+TSA+MG132 (for both CB1 and CB2); p<0.001 IL-1 versus IL-1+TSA and IL-1+TSA versus IL-1+TSA+MG132 (for both CB1 and CB2).

Altogether, these data strongly suggest that NF-κB is involved in cannabinoid receptor induction by GEM with a ROS-independent mechanism.

To verify if the cannabinoid receptors induction by GEM has a role in the synergy, we used 1 μM BAY and 100 nM MG132. Figure 24 shows that both NF-κB inhibitors are able to significantly reduce the antiproliferative synergism by all three combined treatments in Panc1 cells.
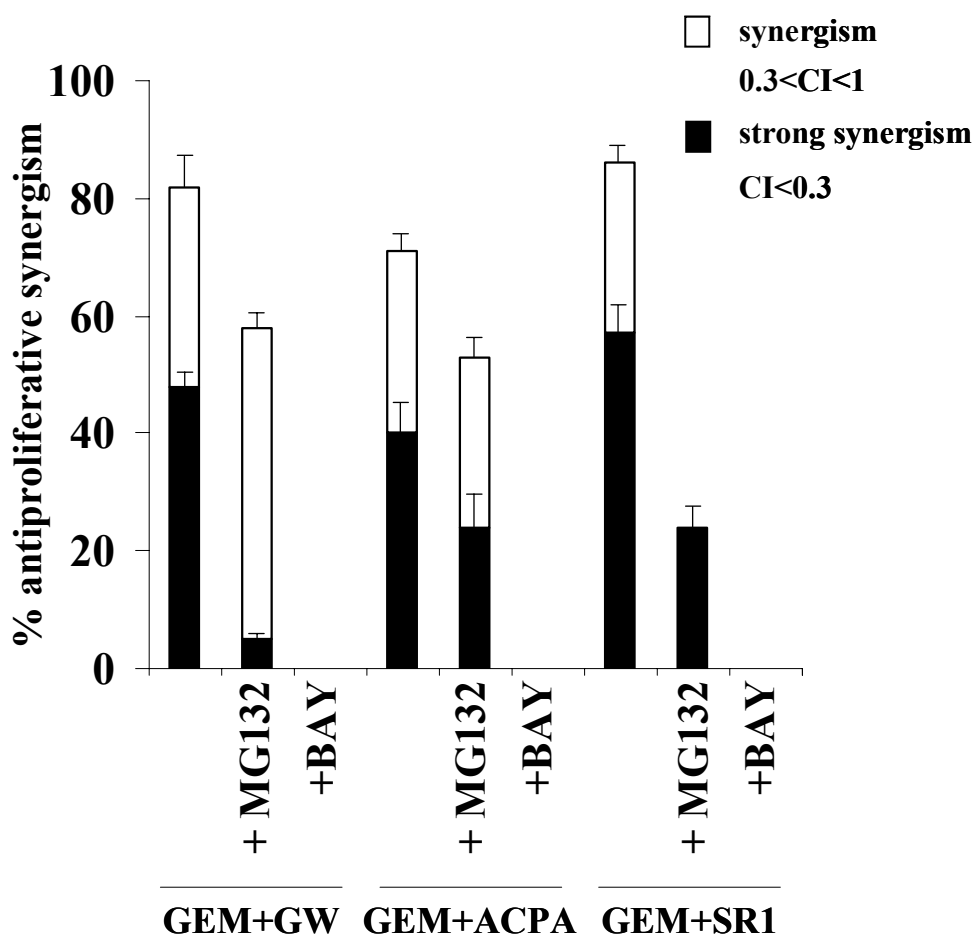
Figure 24: Analysis of the antiproliferative synergism by 2 μM GEM and 40 μM GW, 225 μM ACPA, or 40 μM SR1, in the absence or presence of 100 nM MG132 or 1 μM BAY. Values are the means of three independent experiments (±SD). Statistical analysis for total synergism ($0.3 < CI < 1$): $p < 0.001$ GEM+GW versus GEM+GW+BAY, $p < 0.001$ GEM+ACPA versus GEM+ACPA+BAY and $p < 0.001$ GEM+SR1 versus GEM+SR1+MG or GEM+SR1+BAY; $p < 0.05$ GEM+GW versus GEM+GW+MG and $p < 0.05$ GEM+ACPA versus GEM+ACPA+MG. Statistical analysis for high synergism ($CI < 0.3$): $p < 0.001$ GEM+GW versus GEM+GW+MG or GEM+GW+BAY and $p < 0.001$ GEM+SR1 versus GEM+SR1+BAY; $p < 0.01$ GEM+ACPA versus GEM+ACPA+BAY and $p < 0.01$ GEM+SR1 versus GEM+SR1+BAY; and $p < 0.05$ GEM+ACPA versus GEM+ACPA+MG.

These data indicate that NF-κB is involved in cannabinoid receptor induction by GEM with a ROS-independent mechanism and in the antiproliferative synergism by GEM/cannabinoids, suggesting a role for CB1 and CB2 activation by GEM in the latter effect..

GEM enhances cannabinoid-induced ER stress

It was described that ER stress is a molecular mechanism involved in cannabinoid antiproliferative effect [17]. To investigate whether GEM was able to enhance the cannabinoid-induced ER stress we analyzed XBP-1, Grp78, and CHOP mRNA expression. We show that XBP-1(S), Grp78, and CHOP mRNA levels were increased by GW, ACPA, or SR1 and, although GEM alone was ineffective, they were further significantly enhanced by the addition of GEM (figure 25).
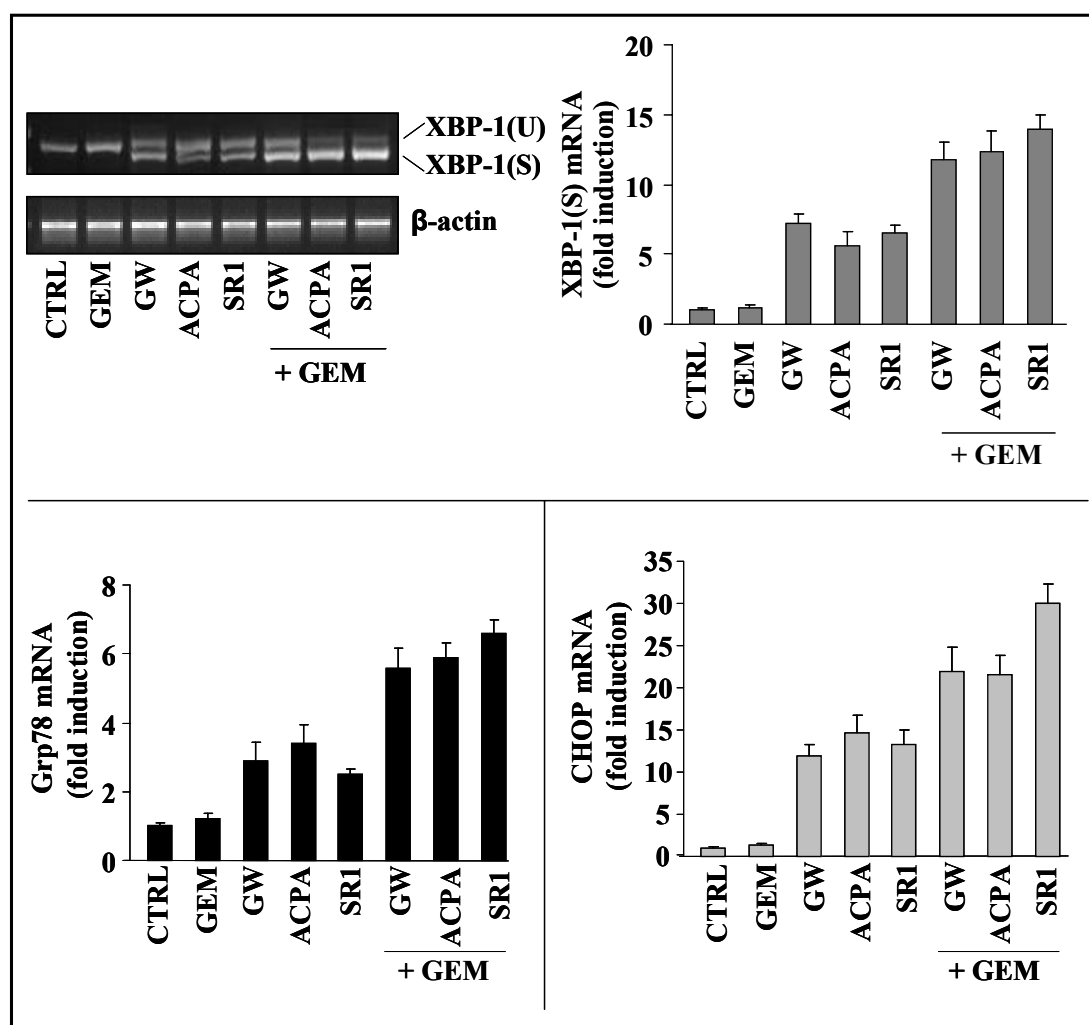

Figure 25: Effect of GEM and/or cannabinoids on ER stress-related genes in Panc1 cells. Cells were treated with 500 nM GEM and/or 40 µM GW, 225 µM ACPA, or 40 µM SR1 for 8 h. Values are the means of triplicate samples from three independent experiments (±SD). p<0.001 GEM versus each cannabinoid; p<0.001 each cannabinoid versus its combination with GEM (for all three genes).

GEM/cannabinoid combination's effect on apoptosis and cell cycle

It has been demonstrated that GEM or cannabinoids can induce the apoptotic cell death program and a cytostatic mechanism [36]. To determine whether apoptosis and cell cycle arrest are involved in the antiproliferative synergism between GEM and cannabinoids, we performed annexin V-FITC/propidium iodide assay and cell cycle analysis by flow cytometry after single or combined treatments. Cells were treated with 200 nM GEM and/or 16 μM GW, 90 μM ACPA, or 16 μM SR1 for 48 h and analyzed by flow cytometry.

Figure 26 shows that at 48 h GEM, but not cannabinoids, significantly induced apoptosis while this effect was partially reduced by the addition of cannabinoids in Panc1 cells. Similar results were obtained at 24 h and in PaCa44 and T3M4 cell lines.
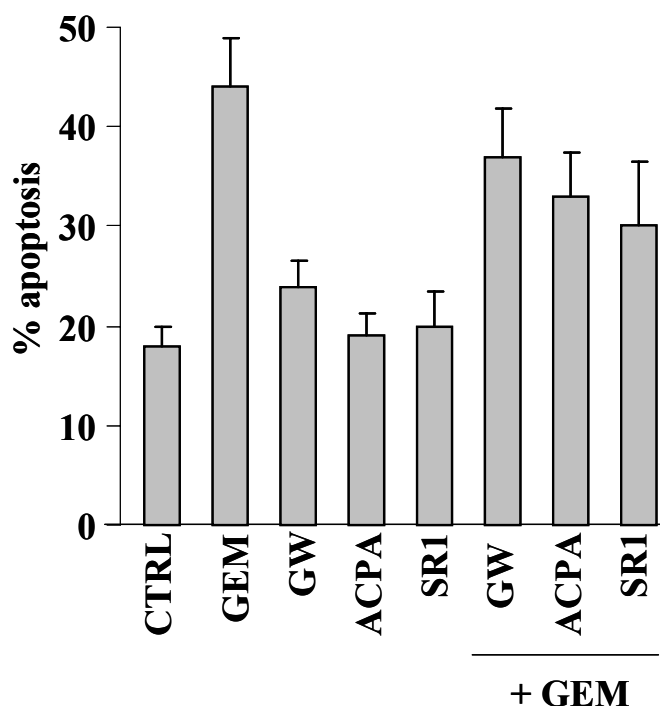

Figure 26: Analysis of apoptosis by GEM and/or cannabinoids in Panc1 cells. Cells were treated with 200 nM GEM and/or 16 μM GW, 90 μM ACPA, or 16 μM SR1 for 48 h and analyzed by flow cytometry to determine the percentages of apoptotic cells. Values are the means of three independent experiments (±SD). $p < 0.001$ control versus GEM; $p < 0.05$ control versus each combination; $p < 0.01$ GEM versus each combination. No significance was observed between control and each cannabinoid.

Figure 27 and table 3 shows that GEM increased the percentages of cells in G1 and S phases and cannabinoids in G1 phase, and the combined treatments did not induce a potentiation of the accumulation of cells in a particular phase of cell cycle when compared with the changes induced by GEM or cannabinoids alone.
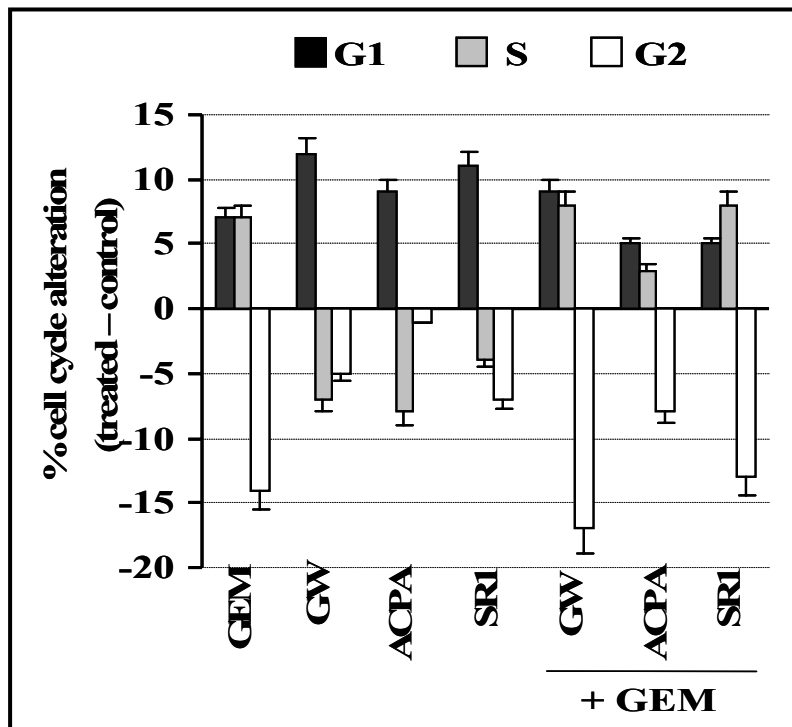

Figure 27: Analysis of cell cycle by GEM and/or cannabinoids in Panc1 cells. Cells were treated with 200 nM GEM and/or 16 µM GW, 90 µM ACPA, or 16 µM SR1 for 48 h. Cell cycle distribution was analyzed by a flow cytometer after DNA staining with propidium iodide. Values are the means of three independent experiments (±SD). No significance was observed between GEM or each cannabinoid versus their combinations.

	cell cycle phase		
	G1	**S**	**G2**
CTRL	45%	22%	33%
GEM	52%	29%	19%
SR1	56%	18%	26%
GEM + SR1	50%	30%	20%
ACPA	54%	14%	32%
GEM + ACPA	50%	25%	25%
GW 405833	57%	15%	28%
GEM + GW 405833	54%	30%	16%

Table 3: Effect of gemcitabine and/or cannabinoids on cell cycle distribution in Panc1 cell line.

Altogether these data indicate that GEM/cannabinoid synergism was not mediated by either an apoptotic or a cytostatic event.

GEM enhances cannabinoid-induced autophagy by a ROS-mediated mechanism

Recently, it has been reported [17] that THC is able to induce autophagy-mediated cell death in human glioma cells. We therefore investigated whether also GW, ACPA, or SR1 were able to induce autophagy and whether this effect could be further enhanced by GEM. Cells were treated with 500 nM GEM and/or 40 μM GW, 225 μM ACPA, or 40 μM SR1 for 24 h in the presence of acid lysosomial protease inhibitors E64d (10 μM) and pepstatin A (10 μg/ml). Interestingly, figure 28 and 29 shows that LC3-II protein, the phospho-ethanolaminated form of the autophagosome protein LC3-I, was induced by GEM or the cannabinoids alone and that it was further significantly enhanced by the combined treatments at 24 h. Similar results were

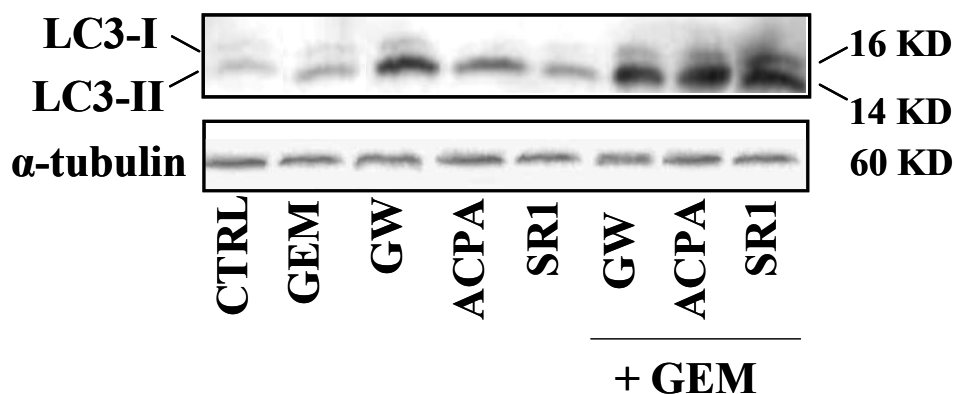observed at 48 h. These data reveal that GEM was able to potentiate the cannabinoid-induced autophagic event.

Figure 28: Analysis of autophagy in Panc1 cells treated with GEM/cannabinoids. Western blot analysis of LC3 was performed using total protein extracts from Panc1 cells treated with 500 nM GEM and/or 40 µM GW, 225 µM ACPA SR1, or 40 µM SR1 for 24 h in the presence of acid lysosomial protease inhibitors E64d (10 µM) and pepstatin A (10 µg/ml). Similar data were obtained after 48 h treatments.
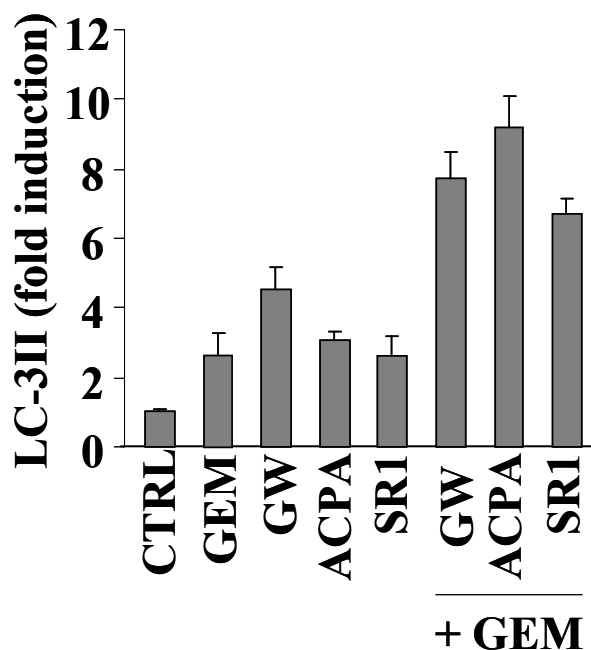

Figure 29: Densitometric analysis of LC3-II bands normalized to α-tubulin. Values are the means of three independent experiments. Statistical analysis: p<0.01 control versus GW or ACPA, p<0.05 control versus SR1, p<0.01 each cannabinoid versus its combination.

Figure 30 shows that the addition of 20 mM NAC to the combined treatments significantly reduced LC3-II expression indicating that oxidative stress is involved in the autophagic event induced by GEM/cannabinoids.
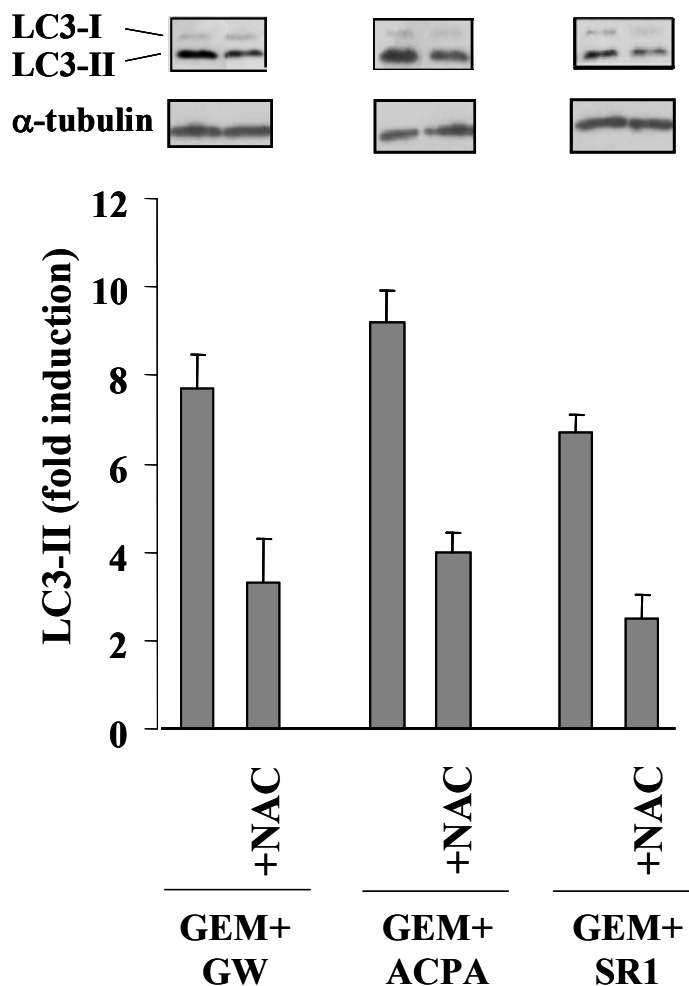

Figure 30: Analysis of autophagy by 500 nM GEM and 40 μM GW, 225 μM ACPA, or 40 μM SR1, in the absence or presence of 20 mM NAC. Values are the means of three independent experiments (±SD). p<0.001 GEM/cannabinoids versus GEM/cannabinoids+NAC.

A late step in the autophagic cell death process is the fusion of lysosomes with autophagosomes into autolysosomes, which can be detected by measuring their acidification with acridine orange staining. Figure 31 show that acridine orange staining (characterized by a punctuature suggesting vacuole formation) slightly increased in GEM-treated cells and significantly potentiated in cells treated with

GEM/cannabinoids combinations and that these effects were almost completely antagonized by the addition of either the scavenger NAC or the autophagy inhibitors 3-methyladenine (3-MA), an inhibitor of the class III phosphatidylinositol 3-kinase (class III PI3K) complex involved in initial autophagosome formation and the lysosomal hydrolasis inhibitor clorochine (CQ).
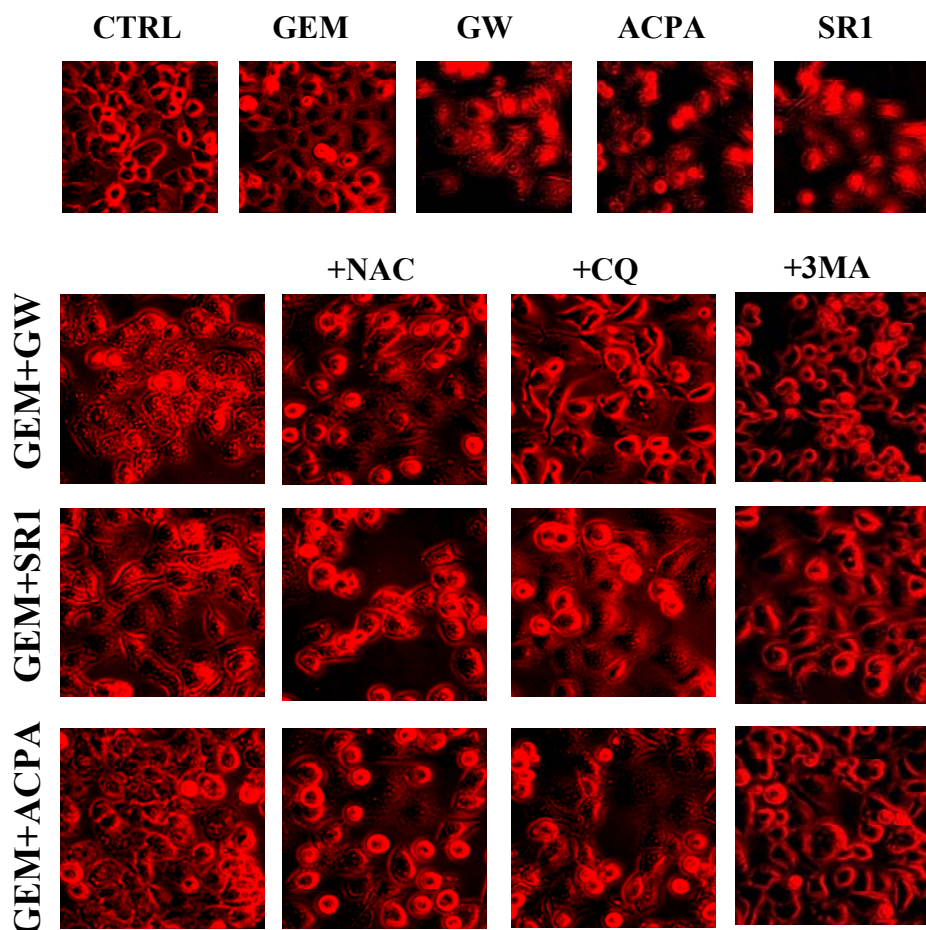

Figure 31: Fluorescence microscopy analysis of autophagosomes formation in Panc1 cells after acridine orange staining treated with 500 nM GEM and 40 µM GW, 225 µM ACPA, or 40 µM SR1, in the absence or presence of 20 mM NAC or10 µM CQ or 1mM 3MA for 24 h.

This observation was quantified and confirmed by FACS analyses and illustrates a significant difference in the acidification of the acidic vesicular organelles (AVOs) in GEM and GEM/cannabinoids combination-treated pancreatic cancer cells. Blocking autophagy with 3-MA or CQ resulted in a decrease in autolysosomal acidification,

demonstrating that acidification induced by the different combinations was linked to the autophagic pathway (figure 32).
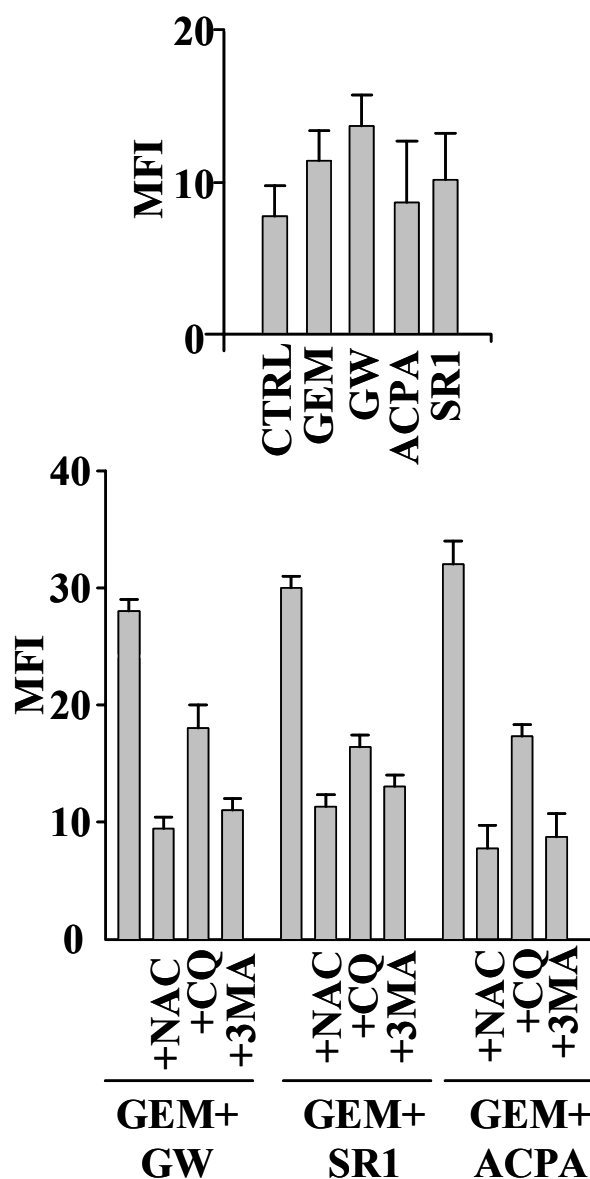
Figure 32: Mean fluorescence intensities (MFIs) were calculated FACS after trypsinization of the acridine orange labelled cells. Values are the means of triplicate samples from three independent experiments (±SD). Statistical analysis: p<0.05 control versus GEM, GW, ACPA, or SR1, p<0.001 each cannabinoid or GEM versus their combination, p<0.001 GEM/cannabinoids versus GEM/cannabinoids+ NAC, GEM/cannabinoids+ CQ or GEM/cannabinoid+3-MA.

To ascertain if the presence of numerous cytoplasmic vacuoles in GEM/combination-treated cells was really due to the induction of autophagy, the autofluorescent drug monodansylcadaverine (MDC), a selective marker for AVOs. The quantitative evaluation of MDC staining performed by FACS. We have found again that GEM, SR1 and ACPA induced a similar increase of AVO formation that was more prominent in GW-treated cells and this effect was strongly potentiated by the GEM/cannabinoids combinations. Again the addition of the autophagy inhibtors CQ or 3MA or the scavenger NAC antagonized this effect (figure 33).
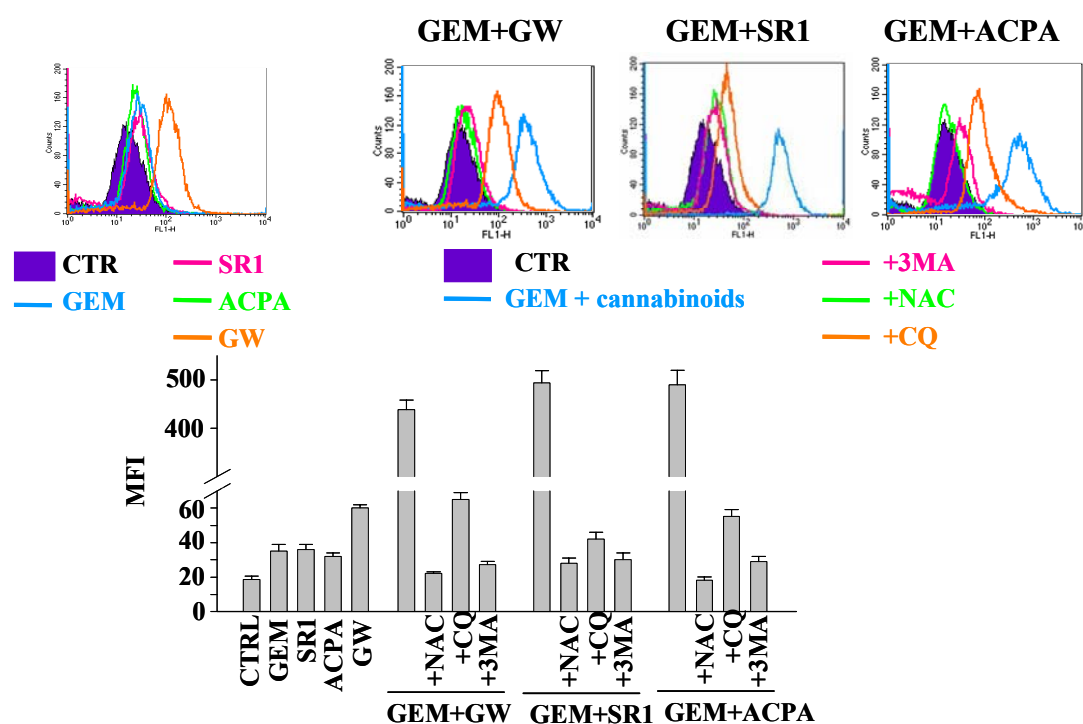
Figure 33: Flow cytometric analyses of autophagosomes formation (MDC incorporation) in Panc1 cells treated with 500 nM GEM and 40 µM GW, 225 µM ACPA, or 40 µM SR1, in the absence or presence of 20 mM NAC or 10 µM CQ or 1mM 3MA for 24 h. Values are the means of three independent experiments (±SD). Statistical analysis: $p < 0.01$ control versus GEM, SR1, or ACPA, $p < 0.001$ control versus GW, $p < 0.001$ each cannabinoid or GEM versus their combination, $p < 0.001$ GEM/cannabinoids versus GEM/cannabinoids+NAC, GEM/cannabinoids+CQ, or GEM/cannabinoid+3-MA.

To test if the GEM/cannabinoids antiproliferative synergism was due to autophagy, we used again 3-MA and CQ. The analysis of antiproliferative synergism was made with 500 nM GEM and 40 μM GW, 225 μM ACPA, or 40 μM SR1 in the absence or presence of 2,5 mM 3-MA or 10 μM CQ. Both 3-MA or CQ strongly reduced the percentages of the antiproliferative synergism (figure 34).
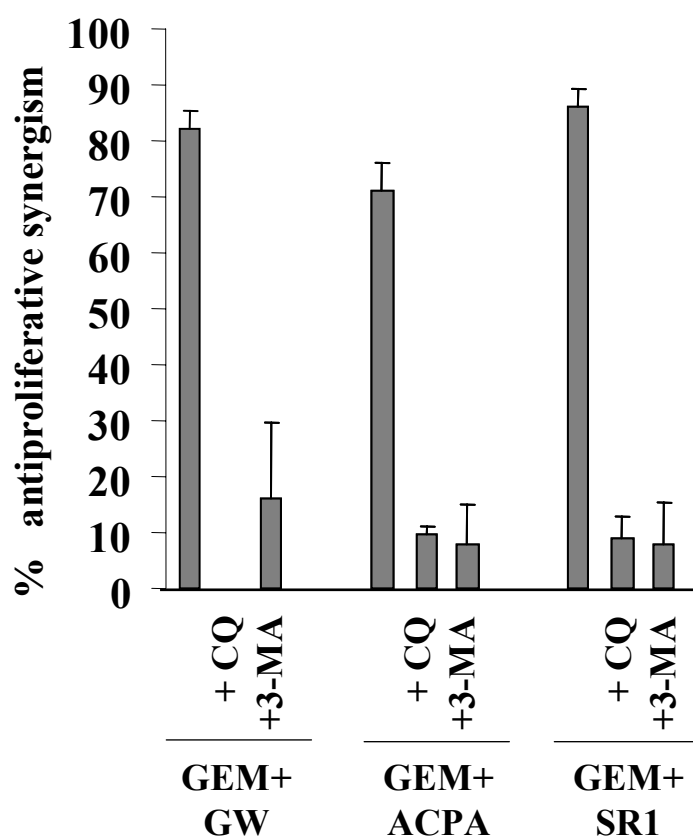
Figure 34: Role of autophagy in the antiproliferative synergism by GEM/cannabinoids in Panc1 cells. The analysis of antiproliferative synergism was made with 500 nM GEM and 40 μM GW, 225 μM ACPA, or 40 μM SR1, in the absence or presence of 2,5 mM 3-MA or 10 μM CQ. Values are the means of three independent experiments (±SD). $p < 0.001$ GEM/cannabinoids versus GEM/cannabinoids+3-MA or GEM/cannabinoids+CQ.

Altogether these data demonstrate that GEM further enhanced cannabinoid-induced autophagy by a ROS-mediated mechanism and that this event is required for GEM/cannabinoid synergism.

A kinetic analysis of the events involved in GEM/cannabinoid antiproliferative synergism shows that oxidative stress, ER stress, and autophagy occurred in different time-points after the beginning of the treatment. Indeed, Figure 35 shows that ROS were induced within 4 h, while the peak of Grp78 and LC3-II protein expression appeared at 8 h and 16 h, respectively, suggesting that ER stress could be a join mechanism between ROS induction and autophagic cell death.
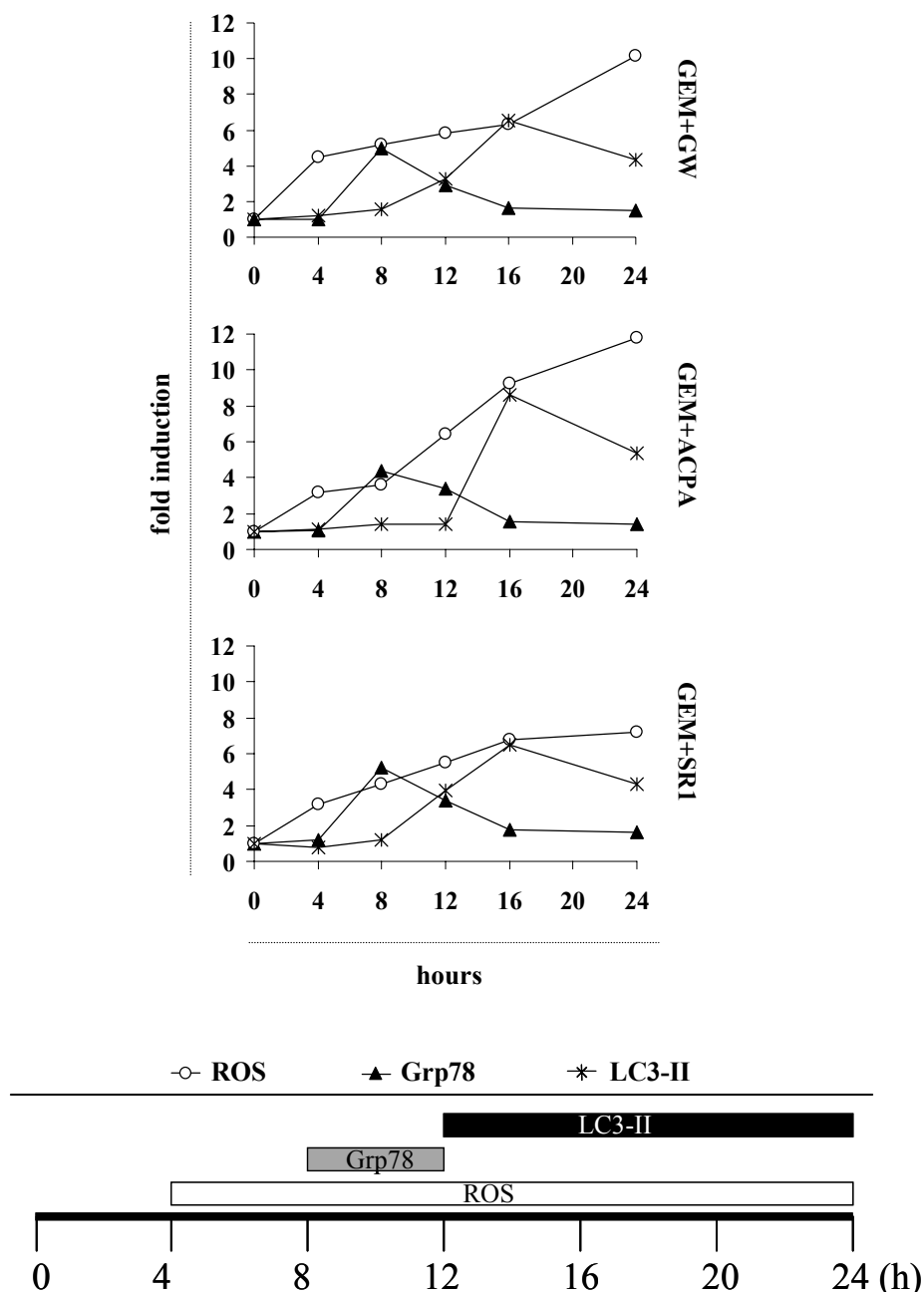

Figure 35: Kinetic analysis of induction of ROS, Grp78, and LC3-II by GEM/cannabinoids in Panc1 cells. Cells were treated with 500 nM GEM and 40 μM GW, 225 μM ACPA, or 40 μM SR1 for the indicated time points. Values are the means of three independent experiments.

GEM and cannabinoids synergistically inhibit growth of human pancreatic adenocarcinoma cells in vivo

For in vivo studies we chose SR1, in addition to GEM, on the basis of its clinical relevance [37]. PaCa44 cells were subcutaneously injected into female nude mice. After 1 week, intraperitoneal injection with PBS (solution vehicle), 25 mg/Kg GEM, or/and 0.28 mg/Kg SR1 were carried out twice a week for 4 weeks. The volume of the tumor in mice treated with the combination GEM+SR1 failed to enlarge, while it increased considerably in the control and, at a lower extent, after GEM or SR1 single treatments. The mice body masses did not change during the experiment, suggesting that the treatments did not produce any apparent toxicity (figure 36).
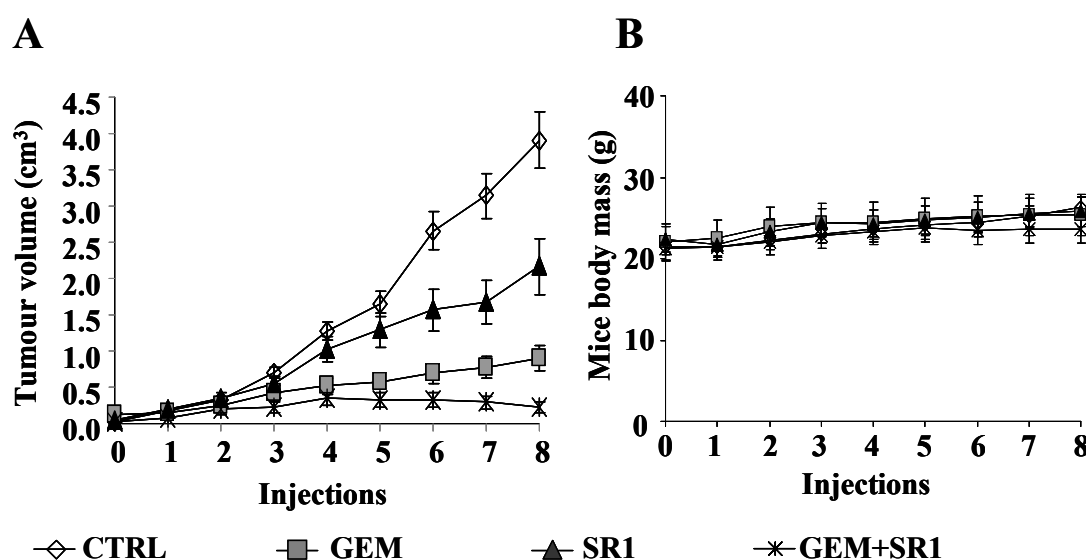
Figure 36: Effect of GEM+SR1 on xenografts of PaCa44 cells in nude mice. PaCa44 cells were subcutaneously injected into female nude mice. After 1 week, i.p. injections with PBS (solution vehicle), GEM, or/and SR1 were carried out twice a week for 4 weeks. (**A**) Values are the means of mice tumour volume measured 3 days after each injection. (**B**) Values are the means of mice body mass measured 3 days after each injection.

At the end of the treatment period, the percentages of mean tumour mass reduction were 65%, 34%, or 92% in mice treated with GEM, SR1, or GEM+SR1, respectively (figure 37).

Figure 37: values of mean tumour mass reduction.
Values are the means of mice tumour mass (±SD)
measured after 8 injections.

It is noteworthy that GEM+SR1 combination determined a quite total inhibition of tumour growth, as representatively shown in figure 38.

Figure 38: Representative photography of tumour masses derived from mice treated with the indicated drugs after 8 injections.
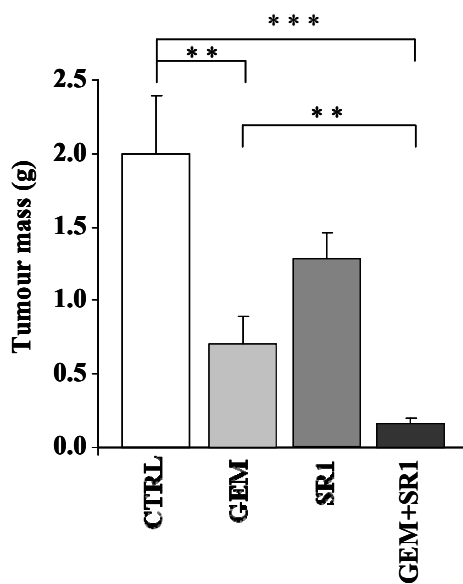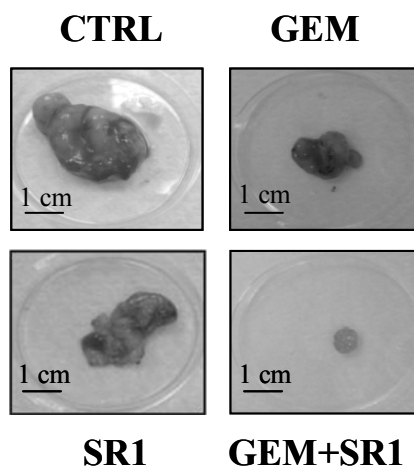
Discussion

Discussion

In the present study, we have demonstrated that the combination between the standard chemotherapeutic agent GEM and cannabinoids synergistically inhibits pancreatic adenocarcinoma cell growth by a ROS-dependent induction of autophagy. We used highly specific cannabinoid ligands of CB1 receptor (ACPA) and of CB2 receptor (GW405833), and the clinically relevant CB1 ligand SR1. The latter has been described as a CB1 antagonist or inverse agonist [38], however, at high concentration it possesses an agonist activity [39]. Our results were in agreement with the last observation and additionally confirmed the dual and concentration-dependent effect of SR1 on cell response (data not shown). It has been demonstrated that SR1, when applied at low concentration, increases the Ca^{2+} current [40], which is generally inhibited by a constitutive endocannabinoid-independent activity of CB1 [41]. Because of its ability to block CB1, which controls food intake at central and peripheral level, SR1 has been adopted for the treatment of obesity and its metabolic complications, including type 2 diabetes, and atherosclerosis [42]. Besides those properties, SR1 has also been shown to exert antitumoral activity in rat thyroid cancer cell lines (KiMol) and in thyroid tumor xenografts [43]. Interestingly, it has recently been reported that SR1 has a stronger antiproliferative activity on the highly invasive metastatic MDA-MB-231 cells than in the less-invasive T47D and MCF-7 cells [44]. In contrast to SR1, to our knowledge, the antitumor activity of ACPA and GW has never been reported before. Thus, our results show for the first time that SR1, ACPA, or GW are able to strongly inhibit pancreatic adenocarcinoma cell growth and to enhance the antiproliferative activity of GEM. To investigate if the synthetic cannabinoids SR1, ACPA, and GW were able to enhance cell growth inhibition induced by GEM we performed dose-dependent analyses of cell viability on six pancreatic adenocarcinoma cell lines: Panc1, PaCa3, PaCa44, T3M4, MiaPaCa2 and CFPAC1. These cell lines have a different sensitivity to GEM: Panc1, PaCa44 and PaCa3 are more resistant, while T3M4, MiaPaCa2 and T3M4 are more sensitive. We have demonstrated that the antiproliferative effect of the combination GEM/cannabinoids, as compared to single-drug treatments, was stronger in GEM-resistant than in GEM-sensitive cell lines. By inverting the molar ratios of the

compounds between the two groups of cell lines, no significant alteration of the results was observed, indicating that the differential behaviour was not due to the specific experimental conditions tested. To evaluate whether cell growth inhibition by GEM/cannabinoids was synergistic, we analyzed the cell viability curves by using the dedicated software CalcuSyn: all combinations gave rise to a significant synergistic reduction of cell viability but the GEM resistant cell lines show a significant higher level of strong synergism compared to the GEM sensitive cell lines. Our data also demonstrate that low doses of GEM/cannabinoids for a treatment period of 24 h are able to significantly reduce pancreatic adenocarcinoma cell growth at least up to 6 days from the beginning of the treatment. This result may be clinically relevant suggesting the possibility to set up therapeutic protocols for pancreatic cancer with low doses of GEM/cannabinoids that could give reduced eventual side effects. Our data also show that cannabinoids were quite ineffective on normal fibroblasts and combined treatments with GEM did not further increase cell growth inhibition. These results are in agreement with the observations that cannabinoid receptors are overexpressed in cancer cells while are undetectable or expressed at low levels in normal cells [36] and that GEM is selectively active in cancer cells which generally show a higher growth rate as compared to normal counterpart. Analysis of ROS is a key element in this project, in fact our research group has reported that pancreatic adenocarcinoma cell growth is strongly inhibited by ROS-inducing compounds [12, 45]. Moreover, we have demonstrated that pancreatic adenocarcinoma cell growth inhibition by GEM is due, at least in part, to ROS induction and that cell lines with a lower basal level of ROS are more resistant to GEM compared to cells with higher ROS levels [11]. In fact, a 4h treatment with GEM/cannabinoids on Panc1 (a resistant cell lines) induces of about two fold ROS production compared to single treatments, while T3M4 (a sensitive cell line) shows no difference in ROS production. Similar results were obtained after 16 h or by inverting the molar ratios of the compounds between the two cell lines. Then, the further induction of ROS by the combined treatment is required for their synergism. This mechanism is supported by the observation that the radical scavenger NAC addition totally inhibits the synergistic antiproliferative effect induced by GEM/cannabinoids. These findings strongly support the idea that the increase of

ROS production may be a good strategy to overcome GEM resistance in the therapeutic management of pancreatic cancer.

It has been previously described that cannabinoid receptor overexpression can potentiate cannabinoid antitumor effect [46]. Here, we report for the first time that GEM treatment determines CB1 and CB2 receptor gene induction, suggesting an involvement of this phenomenon on GEM/cannabinoid synergism. The regulation of CB1 and CB2 gene expression is currently poor studied. Recently, Borner et al. demonstrated that STAT6 mediates the induction of CB1 gene by IL-4 in T lymphocytes [47]. However, it has never been reported that GEM treatment can activate STAT6, strongly suggesting that CB1 and CB2 gene induction by GEM occurs by a different mechanism. Since NF-κB is one of the most important transcription factors induced by GEM [48], we analyzed CB gene induction by GEM in the presence of NF-κB inhibitors, such as MG132, a proteasome inhibitor that inhibits NF-κB activation by preventing IκB degradation, BAY, that is an inhibitor of cytokine-induced IκB-α phosphorylation, PDTC, an antioxidant which inhibit the activation of NF-κB. Interestingly, we show that CB induction by GEM is totally prevented by these inhibitors and that IL-1, a known inducer of NF-κB, is able to induce CB genes. Similar results were obtained using TNF-α. Since NF-κB induction is described to be mediated by oxidative stress [49], we analyzed CB expression after NAC addition. Our data show that it fails to prevent NF-κB induction indicating that GEM induces CB gene with a ROS-independent mechanism. The molecular mechanism at the basis of NF-κB induction by GEM is still unknown and its clarification needs further investigations. Interestingly, the addition of the histone deacetylase inhibitor TSA strongly enhances the NF-κB-dependent CB gene expression induced by GEM. This effect could be due to histone hyperacetylation of the regulatory region of CB gene enhancing binding of NF-κB. An alternative hypothesis is that TSA is able to induce NF-κB acetylation promoting its transcriptional activation, DNA binding affinity, I-κBα assembly or subcellular localization, as previously described [50]. Our previous papers reported that GEM/TSA determined a strong synergistic inhibition of pancreatic cancer cell growth, both in vitro and in vivo [11]. The present data strongly indicate that

GEM/cannabinoid effect could be further potentiated by addition of TSA, suggesting that this triplicate therapy could be an efficient strategy to inhibit pancreatic cancer cell growth. We have also demonstrated that CB mRNAs induction by GEM was transcriptionally regulated, as indicated by its complete inhibition following actinomycin D treatment.

The involvement of ER stress induction in cannabinoid antiproliferative effect has been already described [36]. According with this observation, we report that the cannabinoids ACPA, GW, and SR1 activate: i) the splicing of XBP-1, a transcription factor that regulates the expression of genes important in the cellular stress response; ii) the gene expression of Grp78, a molecular chaperone located in the lumen of the endoplasmic reticulum that is an abundant protein under all growth conditions, but its synthesis is markedly induced under conditions that lead to the accumulation of unfolded polypeptides in the ER; iii) the gene expression of CHOP, which is the molecular switch inducing apoptotic or autophagic cell death signals [51, 52]. Interestingly, we show that all three ER stress-related genes induced by cannabinoids, including CHOP, are further enhanced by GEM, supporting their involvement in GEM/cannabinoid antiproliferative synergism.

To assess how the combination GEM/cannabinoids are able to synergistically inhibit the pancreatic adenocarcinoma cells proliferation, we analyzed the cell cycle perturbation, apoptosis, and autophagy in the resistant cell line Panc1. It has been reported that THC induces caspase activation in pancreatic tumor cells [36]. In contrast, our data demonstrate that SR1, ACPA, or GW do not induce apoptotic cell death, although they induce cell cycle arrest at the G1 phase. The discrepancy between our results and those of Carracedo et al. [36] may rely on the nature of THC, which is a non-specific cannabinoid receptor agonist, and needs further investigations to be explained. Moreover, our results demonstrate that GEM-induced apoptosis is partially, but significantly prevented by cannabinoids. Since it has been reported that autophagy generally precedes apoptosis [53], one possible explanation may be that the stimulation of autophagy by SR1, ACPA, or GW or by their combination with GEM is so elevated to inhibit the development of the apoptotic cell death program. On the other hand, in line with the recent discovery that THC action induces autophagy-mediated cell death in human glioma cells [17], we describe for

the first time that GW, ACPA, and SR1 are able to induce autophagy in pancreatic cancer cells and that GEM strongly enhances the effect of all three cannabinoids analyzed. In fact, we have demonstrated that the protein LC3-II and the formation of autolysosomes increase following treatment with GEM and/or GW, ACPA, SR1. In addition, we demonstrate that the induction of autophagy by GEM/cannabinoids is significantly inhibited by NAC, thus almost completely preventing the antiproliferative synergism. Similar results are obtained with the lysosomal hydrolysis inhibitor CQ, which determines an accumulation of autophagosome vesicles containing LC3-II protein and 3-MA, an inhibitor of the class III phosphatidylinositol 3-kinase (class III PI3K) complex involved in initial autophagosome formation.

Our kinetic studies reveal that ROS induction by drug combinations precedes the activation of the ER stress marker Grp78, which, in turn, precedes the autophagy marker LC3-II induction. The observation that LC3-II increase is prevented by NAC and that ROS can induce ER stress [54, 55] strongly support the hypothesis that oxidative stress, ER stress, and autophagic cell death are sequential events.

Our results demonstrate that GEM strongly potentiates the pathways involved in pancreatic adenocarcinoma cell death by cannabinoids rather than vice versa. To support this concept, we report that GEM is able to induce both CB1 and CB2 genes, thus stimulating the cannabinoid transduction pathway. In addition, previous studies described that GEM is able to stimulate sphingomyelinase or inhibit neutral ceramidase enhancing intracellular ceramide levels [56]. The regulation of ceramide metabolism by GEM, coupled with the observation that the cannabinoid transduction pathway involves ceramide production [57], which in turn is able to induce oxidative stress [58], may be at the basis of the ROS-dependent synergistic autophagic cell death by GEM/cannabinoid combination. In line with our results, in fact, it has been reported that the addition of sphingomyelin, a ceramide precursor, to GEM is able to synergistically inhibit pancreatic cancer cell growth [59].

For in vivo studies we chose SR1, in addition to GEM, on the basis of its clinical relevance [37]. Our in vivo experiments show that intraperitoneal injections of the combination GEM/SR1 into nude mice bearing a subcutaneous mass of human pancreatic adenocarcinoma cells quite completely inhibit tumour growth. No

apparent form of toxicity in vivo, such as mice death, body mass variations, or other apparent toxicity-related features, was observed in mice treated with the combination GEM/SR1.

In conclusion, data in this thesis provide the first evidence that the combination GEM/cannabinoids exerts a strong synergistic antiproliferative effect on pancreatic adenocarcinoma GEM-resistant cell lines by ROS-dependent mechanisms, while it is scarcely toxic towards normal cells. Furthermore, in vivo studies strongly boost the addition of cannabinoids to GEM in designing new therapeutic strategies for pancreatic cancer treatment.

Bibliography

Bibliography

[1.] Laurent, A., et al., *Controlling tumor growth by modulating endogenous production of reactive oxygen species.* Cancer Res, 2005. **65**(3): p. 948-56.

[2.] Hezel, A.F., et al., *Genetics and biology of pancreatic ductal adenocarcinoma.* Genes Dev, 2006. **20**(10): p. 1218-49.

[3.] Jemal, A., et al., *Cancer statistics, 2004.* CA Cancer J Clin, 2004. **54**(1): p. 8-29.

[4.] Li, J., et al., *Updates of adjuvant therapy in pancreatic cancer: where are we and where are we going? Highlights from the "2010 ASCO Annual Meeting". Chicago, IL, USA. June 4-8, 2010.* JOP, 2010. **11**(4): p. 310-2.

[5.] Ramirez, P.J. and S.M. Vickers, *Current status of gene therapy for pancreatic cancer.* Curr Surg, 2004. **61**(1): p. 84-92.

[6.] Pelicano, H., D. Carney, and P. Huang, *ROS stress in cancer cells and therapeutic implications.* Drug Resist Updat, 2004. **7**(2): p. 97-110.

[7.] Neoptolemos, J.P., et al., *Adjuvant therapy in pancreatic cancer: historical and current perspectives.* Ann Oncol, 2003. **14**(5): p. 675-92.

[8.] Burris, H.A., 3rd, et al., *Improvements in survival and clinical benefit with gemcitabine as first-line therapy for patients with advanced pancreas cancer: a randomized trial.* J Clin Oncol, 1997. **15**(6): p. 2403-13.

[9.] Shore, S., et al., *Review article: chemotherapy for pancreatic cancer.* Aliment Pharmacol Ther, 2003. **18**(11-12): p. 1049-69.

[10.] Valko, M., et al., *Free radicals and antioxidants in normal physiological functions and human disease.* Int J Biochem Cell Biol, 2007. **39**(1): p. 44-84.

[11.] Donadelli, M., et al., *Synergistic inhibition of pancreatic adenocarcinoma cell growth by trichostatin A and gemcitabine.* Biochim Biophys Acta, 2007. **1773**(7): p. 1095-106.

[12.] Donadelli, M., et al., *Increased stability of P21(WAF1/CIP1) mRNA is required for ROS/ERK-dependent pancreatic adenocarcinoma cell growth inhibition by pyrrolidine dithiocarbamate.* Biochim Biophys Acta, 2006. **1763**(9): p. 917-26.

[13.] Guindon, J. and A.G. Hohmann, *The endocannabinoid system and pain.* CNS Neurol Disord Drug Targets, 2009. **8**(6): p. 403-21.

[14.] Alexander, A., P.F. Smith, and R.J. Rosengren, *Cannabinoids in the treatment of cancer.* Cancer Lett, 2009. **285**(1): p. 6-12.

[15.] Ledent, C., et al., *Unresponsiveness to cannabinoids and reduced addictive effects of opiates in CB1 receptor knockout mice.* Science, 1999. **283**(5400): p. 401-4.

[16.] Buckley, N.E., et al., *Immunomodulation by cannabinoids is absent in mice deficient for the cannabinoid CB(2) receptor.* Eur J Pharmacol, 2000. **396**(2-3): p. 141-9.

[17.] Salazar, M., et al., *Cannabinoid action induces autophagy-mediated cell death through stimulation of ER stress in human glioma cells.* J Clin Invest, 2009. **119**(5): p. 1359-72.

[18.] Rosenfeldt, M.T. and K.M. Ryan, *The role of autophagy in tumour development and cancer therapy.* Expert Rev Mol Med, 2009. **11**: p. e36.

[19.] Liang, C., et al., *Autophagic and tumour suppressor activity of a novel Beclin1-binding protein UVRAG.* Nat Cell Biol, 2006. **8**(7): p. 688-99.

[20.] Liang, C., et al., *Beclin1-binding UVRAG targets the class C Vps complex to coordinate autophagosome maturation and endocytic trafficking.* Nat Cell Biol, 2008. **10**(7): p. 776-87.

[21.] Geng, J. and D.J. Klionsky, *The Atg8 and Atg12 ubiquitin-like conjugation systems in macroautophagy. 'Protein modifications: beyond the usual suspects' review series.* EMBO Rep, 2008. **9**(9): p. 859-64.

[22.] Kabeya, Y., et al., *LC3, a mammalian homologue of yeast Apg8p, is localized in autophagosome membranes after processing.* EMBO J, 2000. **19**(21): p. 5720-8.

[23.] Eskelinen, E.L., *Maturation of autophagic vacuoles in Mammalian cells.* Autophagy, 2005. **1**(1): p. 1-10.

[24.] Rutkowski, D.T. and R.J. Kaufman, *That which does not kill me makes me stronger: adapting to chronic ER stress.* Trends Biochem Sci, 2007. **32**(10): p. 469-76.

[25.] Schonthal, A.H., *Endoplasmic reticulum stress and autophagy as targets for cancer therapy.* Cancer Lett, 2009. **275**(2): p. 163-9.

[26.] Kouroku, Y., et al., *ER stress (PERK/eIF2alpha phosphorylation) mediates the polyglutamine-induced LC3 conversion, an essential step for autophagy formation.* Cell Death Differ, 2007. **14**(2): p. 230-9.

[27.] Carra, S., et al., *HspB8 participates in protein quality control by a non-chaperone-like mechanism that requires eIF2{alpha} phosphorylation.* J Biol Chem, 2009. **284**(9): p. 5523-32.

[28.] Talloczy, Z., et al., *Regulation of starvation- and virus-induced autophagy by the eIF2alpha kinase signaling pathway.* Proc Natl Acad Sci U S A, 2002. **99**(1): p. 190-5.

[29.] Ogata, M., et al., *Autophagy is activated for cell survival after endoplasmic reticulum stress.* Mol Cell Biol, 2006. **26**(24): p. 9220-31.

[30.] Ding, W.X., et al., *Linking of autophagy to ubiquitin-proteasome system is important for the regulation of endoplasmic reticulum stress and cell viability.* Am J Pathol, 2007. **171**(2): p. 513-24.

[31.] Wei, Y., et al., *JNK1-mediated phosphorylation of Bcl-2 regulates starvation-induced autophagy.* Mol Cell, 2008. **30**(6): p. 678-88.

[32.] Wei, Y., S. Sinha, and B. Levine, *Dual role of JNK1-mediated phosphorylation of Bcl-2 in autophagy and apoptosis regulation.* Autophagy, 2008. **4**(7): p. 949-51.

[33.] Liang, X.H., et al., *Induction of autophagy and inhibition of tumorigenesis by beclin 1.* Nature, 1999. **402**(6762): p. 672-6.

[34.] Hetz, C., et al., *XBP-1 deficiency in the nervous system protects against amyotrophic lateral sclerosis by increasing autophagy.* Genes Dev, 2009. **23**(19): p. 2294-306.

[35.] Meschini, S., et al., *The plant alkaloid voacamine induces apoptosis-independent autophagic cell death on both sensitive and multidrug resistant human osteosarcoma cells.* Autophagy, 2008. **4**(8): p. 1020-33.

[36.] Carracedo, A., et al., *Cannabinoids induce apoptosis of pancreatic tumor cells via endoplasmic reticulum stress-related genes.* Cancer Res, 2006. **66**(13): p. 6748-55.

[37.] Bifulco, M., et al., *Rimonabant: just an antiobesity drug? Current evidence on its pleiotropic effects.* Mol Pharmacol, 2007. **71**(6): p. 1445-56.

[38.] Xie, S., et al., *The endocannabinoid system and rimonabant: a new drug with a novel mechanism of action involving cannabinoid CB1 receptor antagonism--or inverse agonism--as potential obesity treatment and other therapeutic use.* J Clin Pharm Ther, 2007. **32**(3): p. 209-31.

[39.] Krylatov, A.V., et al., *Cannabinoid receptor antagonists SR141716 and SR144528 exhibit properties of partial agonists in experiments on isolated perfused rat heart.* Bull Exp Biol Med, 2005. **139**(5): p. 558-61.

[40.] Hurst, D.P., et al., *N-(piperidin-1-yl)-5-(4-chlorophenyl)-1-(2,4-dichlorophenyl)-4-methyl-1H-p yrazole-3-carboxamide (SR141716A) interaction with LYS 3.28(192) is crucial for its inverse agonism at the cannabinoid CB1 receptor.* Mol Pharmacol, 2002. **62**(6): p. 1274-87.

[41.] Pan, X., S.R. Ikeda, and D.L. Lewis, *SR 141716A acts as an inverse agonist to increase neuronal voltage-dependent Ca2+ currents by reversal of tonic CB1 cannabinoid receptor activity.* Mol Pharmacol, 1998. **54**(6): p. 1064-72.

[42.] Di Marzo, V., *Play an ADAGIO with a STRADIVARIUS: the right patient for CB1 receptor antagonists?* Nat Clin Pract Cardiovasc Med, 2008. **5**(10): p. 610-2.

[43.] Bifulco, M., et al., *A new strategy to block tumor growth by inhibiting endocannabinoid inactivation.* Faseb J, 2004. **18**(13): p. 1606-8.

[44.] Sarnataro, D., et al., *The cannabinoid CB1 receptor antagonist rimonabant (SR141716) inhibits human breast cancer cell proliferation through a lipid raft-mediated mechanism.* Mol Pharmacol, 2006. **70**(4): p. 1298-306.

[45.] Donadelli, M., et al., *Intracellular zinc increase inhibits p53(-/-) pancreatic adenocarcinoma cell growth by ROS/AIF-mediated apoptosis.* Biochim Biophys Acta, 2009. **1793**(2): p. 273-80.

[46.] Shi, Y., et al., *Cannabinoid 2 receptor induction by IL-12 and its potential as a therapeutic target for the treatment of anaplastic thyroid carcinoma.* Cancer Gene Ther, 2008. **15**(2): p. 101-7.

[47.] Borner, C., et al., *Analysis of promoter regions regulating basal and interleukin-4-inducible expression of the human CB1 receptor gene in T lymphocytes.* Mol Pharmacol, 2008. **73**(3): p. 1013-9.

[48.] Arlt, A., et al., *Role of NF-kappaB and Akt/PI3K in the resistance of pancreatic carcinoma cell lines against gemcitabine-induced cell death.* Oncogene, 2003. **22**(21): p. 3243-51.

[49.] Schoonbroodt, S. and J. Piette, *Oxidative stress interference with the nuclear factor-kappa B activation pathways.* Biochem Pharmacol, 2000. **60**(8): p. 1075-83.

[50.] Quivy, V. and C. Van Lint, *Regulation at multiple levels of NF-kappaB-mediated transactivation by protein acetylation.* Biochem Pharmacol, 2004. **68**(6): p. 1221-9.

[51.] Puthalakath, H., et al., *ER stress triggers apoptosis by activating BH3-only protein Bim.* Cell, 2007. **129**(7): p. 1337-49.

[52.] Rouschop, K.M., et al., *The unfolded protein response protects human tumor cells during hypoxia through regulation of the autophagy genes MAP1LC3B and ATG5.* J Clin Invest. **120**(1): p. 127-41.

[53.] Maiuri, M.C., et al., *Self-eating and self-killing: crosstalk between autophagy and apoptosis.* Nat Rev Mol Cell Biol, 2007. **8**(9): p. 741-52.

[54.] Hayashi, T., et al., *Damage to the endoplasmic reticulum and activation of apoptotic machinery by oxidative stress in ischemic neurons.* J Cereb Blood Flow Metab, 2005. **25**(1): p. 41-53.

[55.] Yokouchi, M., et al., *Involvement of selective reactive oxygen species upstream of proapoptotic branches of unfolded protein response.* J Biol Chem, 2008. **283**(7): p. 4252-60.

[56.] Wu, B.X., Y.H. Zeidan, and Y.A. Hannun, *Downregulation of neutral ceramidase by gemcitabine: Implications for cell cycle regulation.* Biochim Biophys Acta, 2009. **1791**(8): p. 730-9.

[57.] Galve-Roperh, I., et al., *Anti-tumoral action of cannabinoids: involvement of sustained ceramide accumulation and extracellular signal-regulated kinase activation.* Nat Med, 2000. **6**(3): p. 313-9.

[58.] Garcia-Ruiz, C., et al., *Direct effect of ceramide on the mitochondrial electron transport chain leads to generation of reactive oxygen species. Role of mitochondrial glutathione.* J Biol Chem, 1997. **272**(17): p. 11369-77.

[59.] Modrak, D.E., et al., *Synergistic interaction between sphingomyelin and gemcitabine potentiates ceramide-mediated apoptosis in pancreatic cancer.* Cancer Res, 2004. **64**(22): p. 8405-10.